Using altimetry to help explain patchy changes in hydrographic carbon measurements

Keith B. Rodgers, Robert M. Key, Anand Gnanadesikan, Jorge L. Sarmiento, Olivier Aumont, Laurent Bopp, Scott C. Doney, John P. Dunne, David M. Glover, Akio Ishida, et al.

Using altimetry to help explain patchy changes in hydrographic carbon measurements

Keith B. Rodgers,[1] Robert M. Key,[1] Anand Gnanadesikan,[2] Jorge L. Sarmiento,[1] Olivier Aumont,[3,4] Laurent Bopp,[5] Scott C. Doney,[6] John P. Dunne,[2] David M. Glover,[6] Akio Ishida,[7,8] Masao Ishii,[9] Andrew R. Jacobson,[10] Claire Lo Monaco,[3] Ernst Maier-Reimer,[11] Herlé Mercier,[4] Nicolas Metzl,[3] Fiz F. Pérez,[12] Aida F. Rios,[12] Rik Wanninkhof,[13] Patrick Wetzel,[11] Christopher D. Winn,[14] and Yasuhiro Yamanaka[7,15]

Received 1 November 2008; revised 27 April 2009; accepted 2 June 2009; published 18 September 2009.

[1] Here we use observations and ocean models to identify mechanisms driving large seasonal to interannual variations in dissolved inorganic carbon (DIC) and dissolved oxygen (O_2) in the upper ocean. We begin with observations linking variations in upper ocean DIC and O_2 inventories with changes in the physical state of the ocean. Models are subsequently used to address the extent to which the relationships derived from short-timescale (6 months to 2 years) repeat measurements are representative of variations over larger spatial and temporal scales. The main new result is that convergence and divergence (column stretching) attributed to baroclinic Rossby waves can make a first-order contribution to DIC and O_2 variability in the upper ocean. This results in a close correspondence between natural variations in DIC and O_2 column inventory variations and sea surface height (SSH) variations over much of the ocean. Oceanic Rossby wave activity is an intrinsic part of the natural variability in the climate system and is elevated even in the absence of significant interannual variability in climate mode indices. The close correspondence between SSH and both DIC and O_2 column inventories for many regions suggests that SSH changes (inferred from satellite altimetry) may prove useful in reducing uncertainty in separating natural and anthropogenic DIC signals (using measurements from Climate Variability and Predictability's CO_2/Repeat Hydrography program).

Citation: Rodgers, K. B., et al. (2009), Using altimetry to help explain patchy changes in hydrographic carbon measurements, *J. Geophys. Res.*, *114*, C09013, doi:10.1029/2008JC005183.

1. Introduction

[2] An important goal for ocean carbon research is to quantify the rate at which anthropogenic CO_2 is taken up by the global ocean. Significant progress was made using World Ocean Circulation Experiment (WOCE) measurements to describe the large-scale distribution of anthropogenic dissolved inorganic carbon (DIC) in the ocean in the 1990s [*Sabine et al.*, 2004]. The success realized with WOCE measurements motivated the extension of CO_2 sampling into the Climate Variability and Predictability (CLIVAR) CO_2/Repeat Hydrography Program (http://www.clivar.org/carbon_hydro), which involves a resampling of the ocean ever 7–12 years. Although the spatial coverage of Repeat Hydrography is less than WOCE, the hope is that the anthropogenic signal inferred from Repeat Hydrography transects can be extrapolated to the basin and global scale with errors smaller than 0.1 Pg C/yr for each of the three major ocean basins [*Bender et al.*, 2002].

[3] However, comparisons of DIC differences measured along WOCE/Repeat Hydrography transects reveal "patchy" structures with both positive and negative changes as large as 50 μmol/kg [*Sabine et al.*, 2006, 2008; *Wanninkhof et al.*, 2006], regardless of whether differences are analyzed in depth or isopycnal space. For the case where surface water pCO_2 in the extratropics approximately tracks the rate of increase of atmospheric

[1]AOS Program, Princeton University, Princeton, New Jersey, USA.
[2]GFDL, NOAA, Princeton, New Jersey, USA.
[3]LOCEAN, IPSL, Université Pierre et Marie Curie, Paris, France.
[4]LPO, IFREMER, IRD, UBO, CNRS, Plouzane, France.
[5]LSCE, DSM, L'Orme des Merisiers, Gif-sur-Yvette, France.
[6]WHOI, Woods Hole, Massachusetts, USA.
[7]FRCGC, JAMSTEC, Yokohama, Japan.
[8]IORGC, JAMSTEC, Yokohama, Japan.
[9]MRI, Tsukuba, Japan.
[10]CIRES, University of Colorado at Boulder, Boulder, Colorado, USA.
[11]MPI, Hamburg, Germany.
[12]CSIC, Madrid, Spain.
[13]AOML, NOAA, Miami, Florida, USA.
[14]College of Natural and Computational Sciences, Hawaii Pacific University, Kaneohe, Hawaii, USA.
[15]Graduate School of Environmental Earth Science, Hokkaido University, Sapporo, Japan.

0148-0227/09/2008JC005183

CO_2 concentrations, one would expect that thermocline DIC concentrations should increase by approximately 10 μmol/kg/decade. Thus suggests that natural variability in oceanic DIC can be comparable to, and at times substantially larger than, the anthropogenic signal sought by the decadal repeat occupations.

[4] What are candidate mechanisms that may account for the patchy structures revealed in difference plots between WOCE and CLIVAR cruises? How does this complicate the detection of anthropogenic changes in oceanic DIC? Candidate mechanisms include the following: (1) biology (changes in biological processes); (2) ventilation (changes in ventilation rates and/or tracer properties at isopycnal outcrops); (3) physical adjustment (large-scale adjustment in thermocline structure associated with Rossby and Kelvin waves in response to wind stress variations); and (4) mesoscale processes (internal mesoscale variations associated with ocean eddies and fronts). The amplitudes and timescales of these mechanisms in changing upper ocean DIC inventories is not yet well understood.

[5] For O_2 concentrations, *Emerson et al.* [2004] reported large decadal changes in the lower thermocline of the North Pacific using decadal repeat section data. *Deutsch et al.* [2005, 2006] interpreted this to be due to the combined effects of ventilation and physical adjustments. More recently, *Mecking et al.* [2008] have used Repeat Hydrography measurements in the North Pacific to argue that mechanism 3 is dominant for decadal variations in thermocline O_2 concentrations. *Sabine et al.* [2008] have identified decadal DIC concentration changes in the North Pacific, and argued that they are consistent with the decadal changes in the meridional overturning of the shallow subtropical cells reported by *McPhaden and Zhang* [2004].

[6] The importance of ocean circulation in driving interannual DIC variability over the upper 100 m of the ocean was previously demonstrated in the modeling study of *Doney et al.* [2009a]. That work built upon results in a dynamically focused modeling study of variability [*Doney et al.*, 2007], where the prognostic equations for temperature for a model run at noneddying resolution were evaluated term by term to demonstrate the importance of advective (ventilation and adjustment) processes in driving upper ocean thermal variations. The coupled model analysis of *Levine et al.* [2008] also emphasized the importance of changes in ocean circulation for driving biogeochemical variations.

[7] In contrast, our analysis begins with repeat ocean hydrographic measurements, and seeks to link specific changes in oceanic DIC and O_2 concentrations with specific changes in the physical state of the ocean. Models are then used to evaluate the representativeness of the relatively few short-timescale repeat measurements. We hypothesize that Rossby waves play a first-order role in driving variations in column inventories of DIC and O_2. Figure 1 shows an idealized east-west section of the upper ocean with two distinct homogeneous layers, as a function of depth and longitude. The upper layer has low density and DIC concentrations, and the lower layer has higher density and DIC concentrations. The interface between the two layers is shown as a solid curve, and represents the position of the thermocline. The focus here is on the upper 1 km of the ocean, where first baroclinic mode Rossby waves are most important. Local perturbations to the interface depth are associated with local convergence in one layer being compensated by local divergence in the other layer. For an Eulerian (fixed longitude) observer at a point where the interface is relatively deep, the column inventory will be relatively small. As baroclinic Rossby waves and eddies are ubiquitous, they are aliased into the "snapshot" sampling obtained through the WOCE and Repeat Hydrography cruises.

[8] In order to better evaluate how tracer inventories can change in a layered framework, we consider the tracer equation for an isopycnal layer in the ocean interior

$$\underbrace{(\partial/\partial t)(CH)}_{\text{Change}} = \underbrace{\text{Bio}_c - \nabla_h(uHC)}_{\text{Source/Sink Advection}} + \underbrace{F_d^{\text{bot}}(C) - F_d^{\text{top}}(C)}_{\text{Diapycnal Flux}} + \underbrace{\nabla_h K_h H \nabla_h C}_{\text{Lateral Mixing}}, \quad (1)$$

where C is some tracer, H is the layer thickness, Bio_c is the source or sink of the tracer associated with biological cycling, ∇_h represents the along-isopycnal gradient, u is the along-isopycnal velocity, $F_d^{\text{top,bot}}$ are the diapycnal fluxes at the top and bottom of the layer, respectively, and K_h is the along-isopycnal diffusive coefficient. We can decompose the advective terms and rearrange the equations as follows:

$$\underbrace{(\partial/\partial t)(CH)}_{\text{Change}} = \underbrace{\text{Bio}_c}_{\text{Source/Sink}} - \underbrace{uH\nabla_h C + F_d^{\text{bot}}(C) - F_d^{\text{top}}(C) + \nabla_h K_h H \nabla_h C}_{\text{Transport/Mixing}} - \underbrace{C\nabla_h(uH)}_{\text{Convergence/Divergence}}. \quad (2)$$

The inventory of tracer C within a layer can change because of sources or sinks, because water with a different concentration of the tracer advects or mixes into the region, or because the layer is either thickened or thinned. The last term of equation (2) (convergence) will project onto changes in the column inventory of the tracer, as convergence in one layer will be compensated by divergence in another layer as illustrated in Figure 1. Changes in sea surface height (SSH) are approximately 2 orders of magnitude smaller than corresponding changes in the depth of the layer interface. Therefore, although SSH is an indicator of the depth of the layer interface, the contributions of SSH itself to variations in the thickness of the upper layer in Figure 1 are negligible.

[9] The major point of this paper is to evaluate the importance of the convergence term in equation (2) to the natural variability of DIC and O_2 in the ocean. If the convergence term is important, then this information could then be incorporated into methods used for detecting anthropogenic DIC changes in the ocean. Any changes in layer thickness that project onto the first baroclinic mode (associated with the most energetic wind-driven planetary scale waves and ocean eddies) will result in changes in SSH. In that sense an important component of this work is to test the idea that changes in SSH can be used to detect changes in layer thickness. This does not imply that changes in

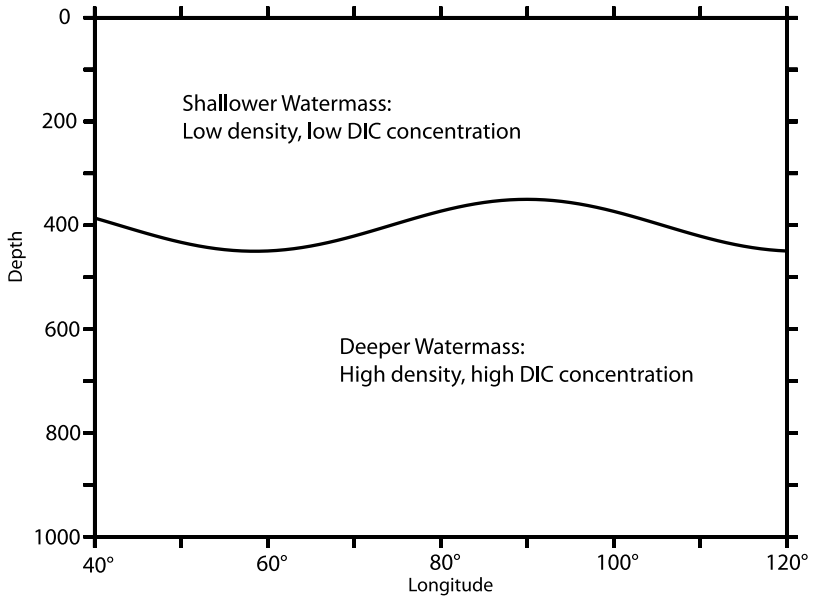

Figure 1. Snapshot schematic of an instantaneous state of a simplified two-layer ocean as a function of longitude and depth, with a lighter upper layer (with relatively low DIC concentrations) being separated from a denser lower layer (with relatively high DIC concentrations). Each layer is assumed to be homogenous in both density and DIC concentration. Perturbations to the interface between the layers is intended to represent the activity of Rossby waves.

ventilation, such as those discussed by *Deutsch et al.* [2005, 2006] and *Mecking et al.* [2008] are unimportant. Understanding ventilation changes is vital to monitoring the carbon cycle and detecting any potential responses to climate change. However, just as such changes in ventilation may obscure the anthropogenic transient signal, they may themselves be masked, particularly on short timescales, by processes that redistribute fluid.

[10] To illustrate how the convergence term in equation (2) can impact column inventories of tracers, we turn our attention to the mean state for three quantities integrated over the upper 1 km of the ocean: DIC, O_2, and dynamic height. Dynamic height is an analog of sea surface height that is calculated from hydrographic measurements (temperature and salinity). These time mean quantities are derived from the annual mean Global Ocean Data Analysis Project (GLODAP) [*Key et al.*, 2004] for natural (preanthropogenic) DIC as well as anthropogenic DIC, the World Ocean Atlas temperature (WOA05 [*Locarnini et al.*, 2006]), salinity [*Antonov et al.*, 2006], and O_2 [*Garcia et al.*, 2006]. We refer to the vertical inventories of DIC and O_2 as DICINV and O2INV, respectively.

[11] Figure 2a shows the local deviation of DICINV from the global mean (color; mol C/m^2), which we shall refer to as anomalous DICINV (ADICINV) and the anomalous dynamic height (contours; m). The ADICINV diagnostic is intended to emphasize the amplitude of the background gradients rather than the absolute values. Large-scale geostrophic flow is generally parallel to dynamic height isolines with stronger flow associated with stronger gradient regions. For many regions, including the frontal regions of the Southern Ocean, the subtropical/tropical boundary region of the North Pacific and the Southern Indian Ocean, and the subtropical/subpolar boundary region of the North Pacific, the strong gradient regions in dynamic height are also gradient regions in ADICINV. The correspondence reflects the fact that the pycnocline structure often corresponds to the nutricline structure and to the distribution of DIC. A notable exception is the North Atlantic, where the density gradients at the subtropical/subpolar frontal boundary are not mirrored in lateral ADICINV gradients.

[12] The relationship between gradients in ADICINV (contours; mol C m^{-2}) and anthropogenic inventories of DIC (colors; mol C m^{-2}) is shown in Figure 2b. Anthropogenic DIC accumulation tends to be large in well-ventilated regions where ADICINV is small. This is of potential importance to the problem of detection, as it means that local maxima in anthropogenic DIC do not tend to coincide with regions where there are large lateral gradients in the mean (in other words, regions where the term $\nabla\overline{C}$ in equation (1) is large). As an example, the maximum in anthropogenic DIC inventory for the Southern Ocean is located near 40°S, whereas the large lateral gradient regions for ADICINV tend to occur near 50°S.

[13] The equivalent field for O_2 (anomalous O2INV (AO2INV)) is shown in Figure 2c (colors; mol C m^{-2}), superposed with dynamic height at the surface relative to a depth of 1 km is (contours; m). For much of the Pacific and Indian Oceans poleward of 20°S, the gradient regions in AO2INV largely mirror the large gradient regions in ADICINV. However, for higher latitude regions of the Southern Ocean and the North Atlantic, the high gradient regions of the two fields (AO2INV and ADICINV) are not coincident. For the North Atlantic, the gradient regions in AO2INV coincide with the dynamical subtropical/subpolar boundary region.

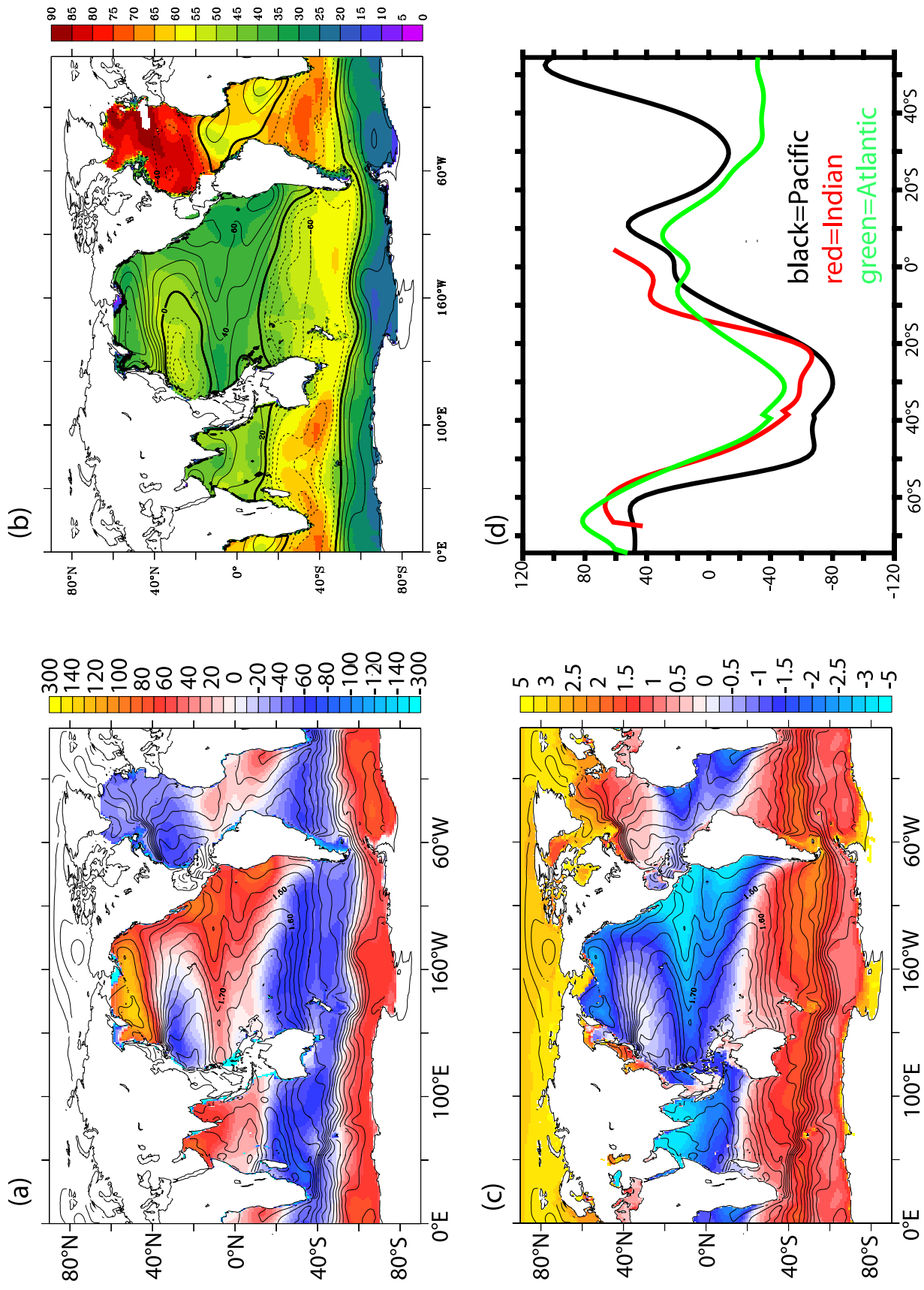
(a)
(b)
(c)
(d)
black=Pacific
red=Indian
green=Atlantic
80°N
40°N
0°N
40°S
80°S
0°E
100°E
160°W
60°W
0°
20°S
60°S
120
80
40
0
-40
-80
-120

Figure 2

[14] Figure 2d shows ADICINV from GLODAP (units of mol C m^{-2}) along a WOCE section from each basin: P16 along 152°W in the Pacific (black), I8 along 80°E in the Indian Ocean (red), and A16 along 20°W in the Atlantic (green). The amplitude of the meridional gradients $\partial(\overline{\mathrm{DICINV}})/\partial y$ can be as large as 10 mol C m^{-2} per 1° latitude. This occurs in regions where the lateral gradient in the anthropogenic perturbation concentration can be an order of magnitude smaller.

[15] In summary, the main goal of this study is to test the idea that there is a correlation between SSH and column inventories of natural DIC, and to identify whether this relation can be applied to the detection of anthropogenic DIC in the ocean. This study makes combined use of both ocean measurements and model simulations using three-dimensional models. From the framework of detection, a characterization and mechanistic understanding of the background "noise" of natural variability has been suggested [*Levine et al.*, 2008] as an important step in reducing the potential uncertainty of empirical multivariate linear regression methods (such as the now widely used the extended multiple linear regression (eMLR) method of *Friis et al.* [2005]). As such, our method is intended to be complementary to such databased detection methods, and to highlight the ways in which the uncertainties in such methods may be reduced.

2. Data Description

[16] We focus on sections that are sampled with timescales significantly shorter than the sampling interval of the repeat hydrography programs. The first is WOCE I8N (at 80°E) in the Indian Ocean, which was sampled in March 1994 [*Johnson et al.*, 1998] and by NOAA in September 1995 [*Peltola et al.*, 1998]. Second is the Observatoire de la Variabilité Interannuelle a Decennale (OVIDE) transect between Spain and Greenland [*Lherminier et al.*, 2007; *Pérez et al.*, 2009] that was sampled in June 2002 and 2004. Third is the Ocean Indien Service d'Observation (OISO) cruises OISO_01 and OISO_03 in December 1997 and January 1999 [*Jabaud-Jan et al.*, 2004; *Metzl et al.*, 2006].

[17] The SSH anomaly (SSHA) data product considered here is from the multimission, merged, and mapped data product available from http://www.aviso.oceanobs.com (hereafter referred to as the Archiving, Validation, and Interpretation of Satellite Oceanographic Data (AVISO) SSHA data product). This data product is composed of measurements from Envisat, ERS, Topex/Poseidon, as well as Jason-1 [*Le Traon et al.*, 2003; *Pascual et al.*, 2006], and the approximate resolution is one week by 40 km. We consider changes in SSHA along the transects corresponding to the in situ ocean measurements.

3. Description of Models

[18] The following five different models are included in this study: (1) Center for Climate SystemResearch (CCSR) Ocean Component Model (COCO)-North Pacific Ecosystem Model for Understanding Regional Oceanography (NEMURO) from the Frontier Research Center for Global Change (FRCGC) in Japan, (2) Max-Planck- Institute ocean model (MPIOM)-Hamburg Model of the Ocean Carbon Cycle (HAMOCC5) from the Max-Planck-Institut (MPI) für Meteorologie in Hamburg, Germany, (3) ORCA2-Pelagic Interaction Scheme for Carbon and Ecosystem Studies (PISCES) from the Institut Pierre Simon Laplace (IPSL) in France, (4) Version 3 of the Community Climate System Model (CCSM3)-Biogeochemical Element Cycling (BEC) from National Center for Atmospheric Research (NCAR), and (5) Modular Ocean Model Version 4 (MOM4)-Tracers in the Ocean with Allometric Zooplankton (TOPAZ) from Geophysical Fluid Dynamics Laboratory (GFDL). For each of the models chosen, two separate runs have been performed. The two runs differ only in their atmospheric boundary condition for CO_2 concentrations. The first used constant preanthropogenic concentrations of 278 μatm, and the second used the atmospheric transient over 1760–2003. For each set of two runs with the same model, the evolution of the physical state variables (temperature, salinity, etc.) is identical, and only the biogeochemical fields differ. Although the models differ in their respective physical and biogeochemistry/ecosystem component models, they were all forced with interannually varying surface fluxes.

[19] The experiment with the atmospheric CO_2 transient is referred to as PRT ("perturbation"), that with constant atmospheric CO_2 as CTL ("control"), and the difference between these two (PRT-CTL) as ANT ("anthropogenic"). COCO-NEMURO is referred to as FRCGC, MPIOM1-HAMOCC5 as MPI, ORCA2-PISCES as IPSL, CCSM3-BEC as NCAR, and MOM4-TOPAZ as GFDL. The horizontal resolution of FRCGC and GFDL is roughly 1°, that of MPI is 3°, that of NCAR is 2°, and IPSL is approximately 2° * cos(latitude) in the extratropics, with enhanced meridional resolution of 0.5° near the equator. More details regarding the models and their respective configurations are given in Appendix A.

4. Results

[20] We first present the results for the observations, and then the results for the models. For the data, we consider the sections mentioned above where relatively high-frequency

Figure 2. Vertical integrals of tracer and hydrographic fields over the upper 1000 m. (a) Deviations of vertical inventories of preanthropogenic (natural) GLODAP DIC [*Key et al.*, 2004] from the global mean (mol C m^{-2}, colors) and dynamic height calculated from World Ocean Atlas (WOA05) temperature [*Locarnini et al.*, 2006] and salinity [*Antonov et al.*, 2006] (m, contours). (b) Column inventory of anthropogenic DIC from GLODAP data product (mol C m^{-2}, colors) and deviations of inventories of preanthropogenic DIC from the global mean (mol C/m^2, contours). (c) Deviations of the vertical inventories of O_2 from WOA05 [*Garcia et al.*, 2006] and dynamic height calculated from WOA05 temperature and salinity. (d) Deviations of inventories of preanthropogenic DIC from mean along sections P16 (152°W in the Pacific, black), I8N (80°E in the Indian, red), and A16 (20°W in the Atlantic, green). Values are in mol C m^{-2}.

repeat measurements are available, on timescales significantly shorter than the resampling timescale of the Repeat Hydrography program. We then turn to the models.

4.1. Observations: Seasonal and Interannual Changes

[21] We now turn our attention to changes in DIC inventories over the upper 1 km (DICINV), O_2 inventories over the upper 1 km (O2INV), and sea surface height (SSH) from AVISO SSHA data product along 80°E in the Indian Ocean (WOCE I8N). Here the sampling interval (6 months) is sufficiently short that there should be very little anthropogenic DIC accumulated over this period with expected column inventory accumulation less than 0.5 mol C m^{-2}. The SSH anomaly (deviation from the mean) from AVISO SSHA data product is shown averaged over March 1995 in Figure 3a and averaged over September 1995 in Figure 3b, and the difference (September minus March) in Figure 3c.

[22] Over 15°N–15°S both March and September 1995 exhibit large and relatively coherent structures of positive and negative SSH anomalies, with more evidence of smaller mesoscale variations poleward of 15° latitude. The large structures represent westward-propagating Rossby waves. Positive anomalies are associated with positive thermocline depth anomalies. Thus for March 1995 along 8°S, the displacement of the thermocline associated with the SSH anomalies in Figure 3a may be expected to roughly correspond to perturbations of the idealized thermocline in Figure 1 (although at 8°S the thermocline should be somewhat shallower than what is represented in Figure 1).

[23] The change in monthly mean SSH (ΔSSH) between March and September 1995 is shown in Figure 3c, and the stations sampled along I8N are overlain as a series of symbols. Between 15°N–15°S, there are large and relatively coherent structures of negative and positive ΔSSH, with more evidence of smaller-structure mesoscale variations poleward of 15° latitude. The largest positive ΔSSH (in excess of 15 cm) is centered near 90°E, 8°S. This feature is significantly larger than the characteristic scale of mesoscale variability (the Rossby Radius is approximately ∼100 km in this region), and is due to westward-propagating Rossby waves. *Perigaud and Delecluse* [1992] established that such Rossby wave activity is an integral part of the seasonal cycle in this region. The remnant of an earlier Rossby wave can be seen in the negative ΔSSH along 80°E between 12°S and 18°S. The maximum positive ΔSSH structure is shifted to the east as one moves poleward, demonstrating that Rossby wave propagation speed decreases with latitude.

[24] Changes in SSH (ΔSSH), DICINV (ΔDICINV), and O2INV (ΔO2INV) along the section are shown in Figure 3d. The mean ΔSSH (2°N–22°S) is −2.84 cm, while the mean ΔDICINV is 3.4 mol C m^{-2}. ΔDICINV is nearly an order of magnitude larger than the expected accumulation of anthropogenic DIC over 6 months. The perturbation to the thermocline structure associated with the Rossby wave activity drives a significant short-timescale perturbation to the DIC distribution. This manifests itself as a change in the mean DIC concentration along the transect. Changes in DICINV are largely mirrored in O2INV. It would be difficult to argue that ΔDICINV and ΔO2INV are driven by nonlocal ventilation changes (mechanism 2 listed in the Introduction), since this would required that local dynamical and local tracer perturbations were coincidentally aligned.

[25] The temporal evolution of SSH anomalies from the AVISO data product is represented as a Hovmoller diagram along 7°S in the Indian Ocean in Figure 3e and along 13°S in Figure 3f. These correspond to the two latitudes for which there were maximum changes in SSH revealed in Figure 3d. The diagrams clearly demonstrate the westward propagation of the SSH anomaly signals over the year 1995. For each of these Hovmoller diagrams, the two dates corresponding to the repeat cruises are marked along 80°E as black squares. Importantly, the diagram reveals that the longitude (80°E) corresponding to the Repeat measurements is representative of the large-scale variations over the Indian Ocean.

[26] Next we examine North Atlantic changes between June 2002 and 2004 along the OVIDE section between Spain and Greenland (Figure 4a). As with I8N, we consider ΔDICINV, ΔO2INV, and ΔSSH from the AVISO SSHA data product corresponding to the OVIDE cruise track. DIC was calculated from pH and alkalinity using the same algorithms that were used as part of the GLODAP project. The time interval between the cruises is only 2 years, so the expected accumulation of anthropogenic DIC should be ∼2 mol C m^{-2}.

[27] ΔSSHA is shown in Figure 4a. In 2002 there was a relatively well-defined dynamical frontal structure centered near 51°N. The change in the vertically integrated tracer quantities along this section are compared with the changes in SSH along the section in Figure 4b. For this section, the change in SSH (ΔSSH) is not reflected in the change in the column inventory of DIC (ΔDICINV). This stands in contrast to what was found for the Indian Ocean (Figure 3d), where there was a much closer correspondence between ΔSSH and ΔDICINV.

[28] For O2INV, on the other hand, there are significant changes that reflect the fact that for the mean a significant concentration front is associated with the dynamical front (Figure 2a). This decoupling between ΔDICINV and ΔO2INV is evidence that the changes are not driven by biology, as if the changes were purely biologically driven both quantities would be expected to change (with opposite sign). For the case of the O2INV changes, arguing that they are driven by nonlocal ventilation changes would require that the correspondence between ΔSSH and ΔO2INV be purely coincidental.

[29] The large-scale dynamical controls on the changes between 2002 and 2004 most importantly reflect the fact that the North Atlantic Current (NAC) was sharper in 2002 than in 2004. At the latitude corresponding to OVIDE, the NAC itself consists of two main branches, the Western NAC (WNAC) and the Eastern NAC (ENAC), and with the region exhibiting energetic eddy variability. The WNAC was located 200 km further to the northwest in 2004 than in 2002, and this accounts for the positive SSH anomaly seen at 52°N in Figure 4. As the thermocline water in the NAC system is lower in O_2 than the water to the northwest of the WNAC, the associated O_2 anomaly is negative. The ENAC was found further to the southeast in 2004 than in 2002. This accounts for the negative SSH anomaly at 48°N. As the thermocline water southeast of the WNAC are of the same subtropical/Mediteranean origin, ther is no oxygen

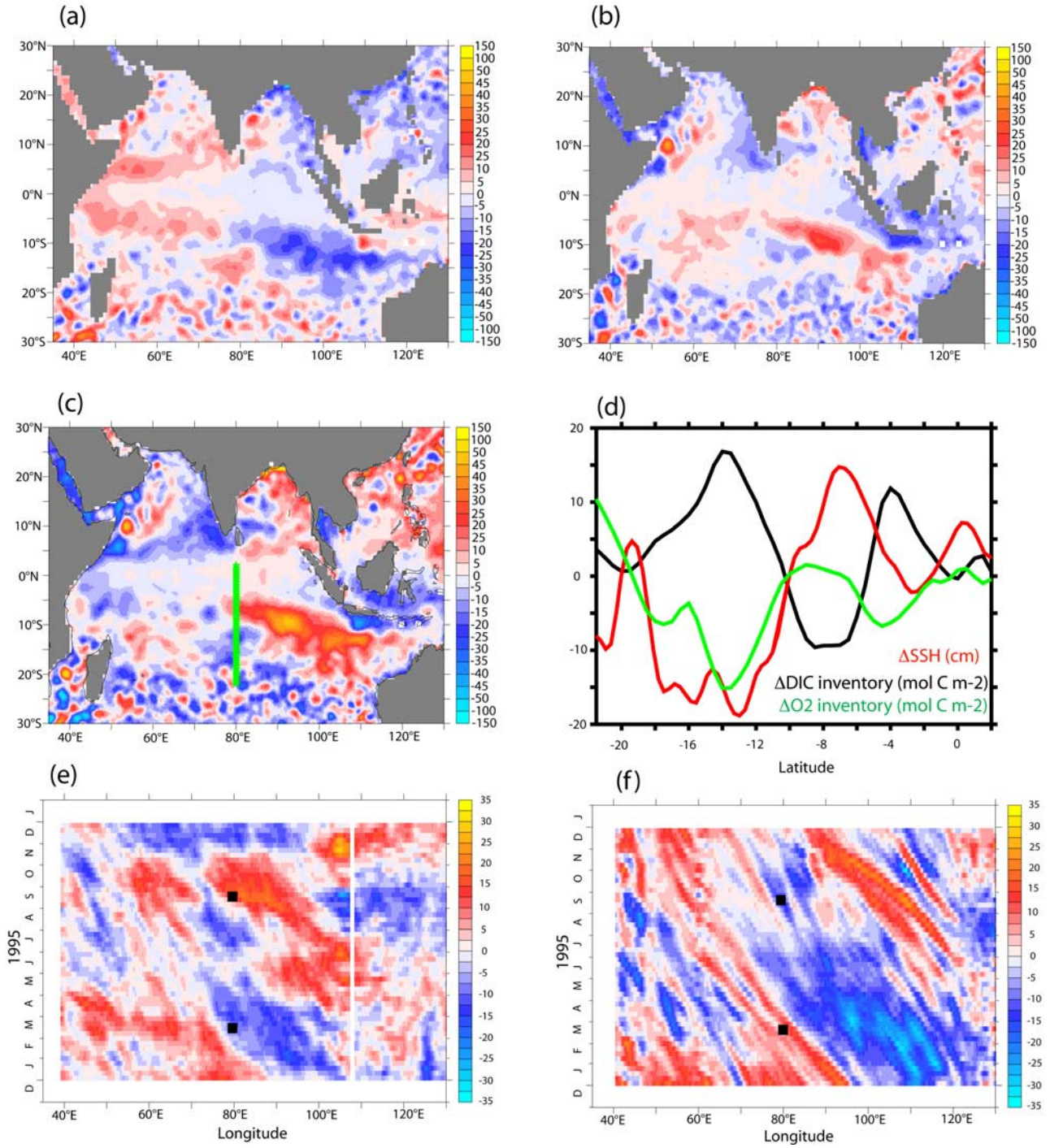

Figure 3. Changes in Indian Ocean between March and September 1995 [*Johnson et al.*, 1998; *Peltola et al.*, 1998]. (a) Sea surface height anomalies from AVISO in March 1995 (cm). (b) Sea surface height anomalies from AVISO in September 1995 (cm). (c) Change in sea surface height from AVISO (September 1995 minus March 1995). (d) Changes in column integral of DIC over upper 1000 m (mol C m^{-2}, black), sea surface height from AVISO (cm, red), and O_2 (green). (e) Evolution of SSH anomalies from AVISO along 7°S in the Indian Ocean during 1995 (cm). (f) Evolution of SSH anomalies from AVISO along 13°S in the Indian Ocean during 1995 (cm).

front there and no significant difference in the O_2 inventory between 2002 and 2004 associated with the change in the SSH front. Again, over this region meridional gradients in DIC concentrations tend to be small, as is reflected in Figure 2d.

[30] We now turn our attention to a third data set, the OISO cruises in the Southern Ocean, which constitute the

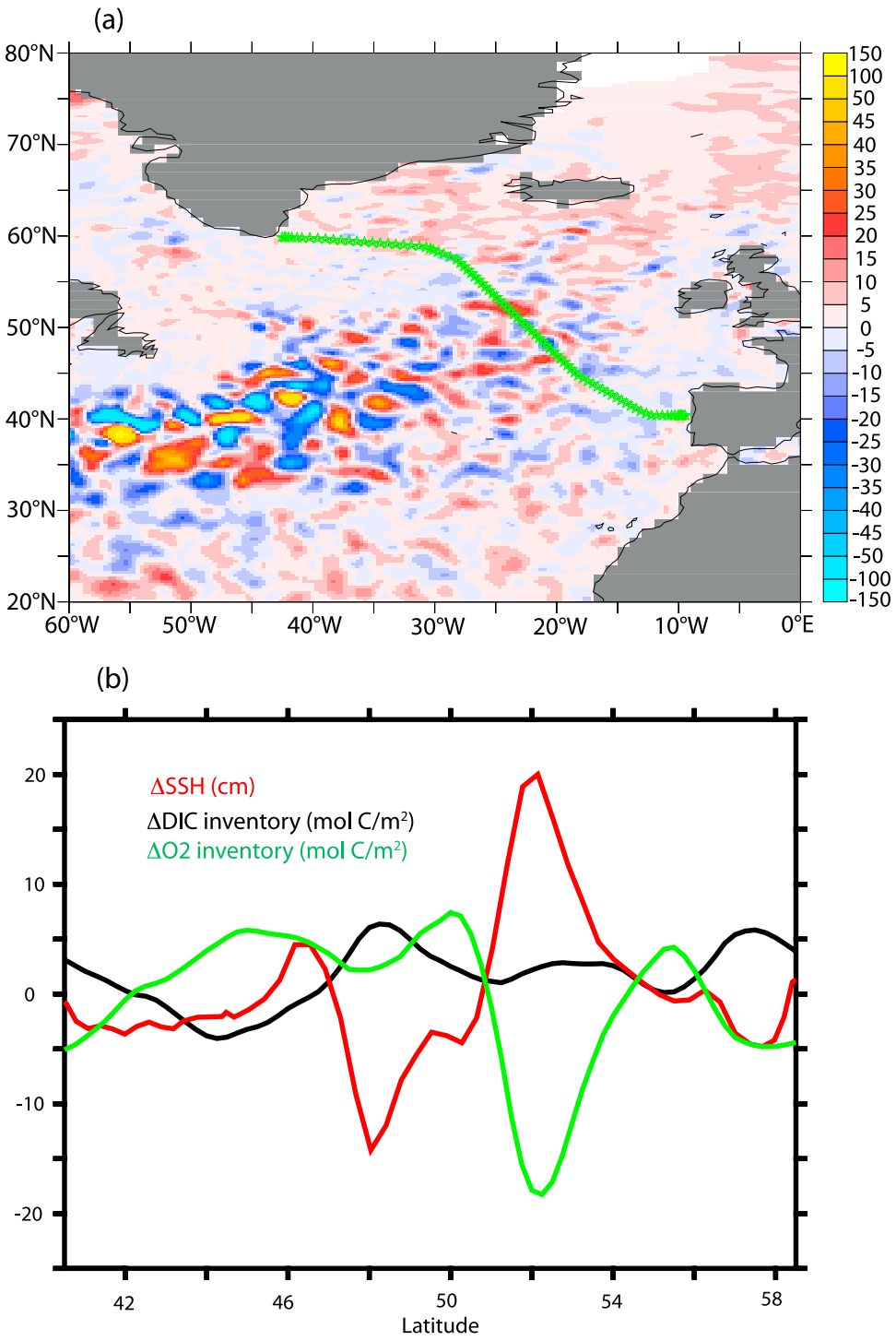

Figure 4. OVIDE in North Atlantic between Spain and Greenland [*Lherminier et al.*, 2007; *Pérez et al.*, 2009]. (a) Changes in vertical inventory of DIC over the upper 1000 m (mol C m^{-2}, black), sea surface height from AVISO (cm, red), and O_2 (green). (b) Change in sea surface height from AVISO (cm, June 2004 minus June 2002).

third data set considered here. Our focus is on the OISO surveys conducted in January 1998 (OISO_01) and December 1998 (OISO_03), as this spans the period of large global changes in ocean circulation associated with the 1997/98 El Niño event. The variables considered here are ΔSSH and ΔDICINV.

[31] The global structure of change in monthly mean SSH from the AVISO SSHA data product between January 1998 and December 1998 shown in Figure 5a reveals large changes in SSH in the tropics, with regions of decreased (increased) SSH reflecting regions where the tropical thermocline has shoaled (deepened). It is known that the

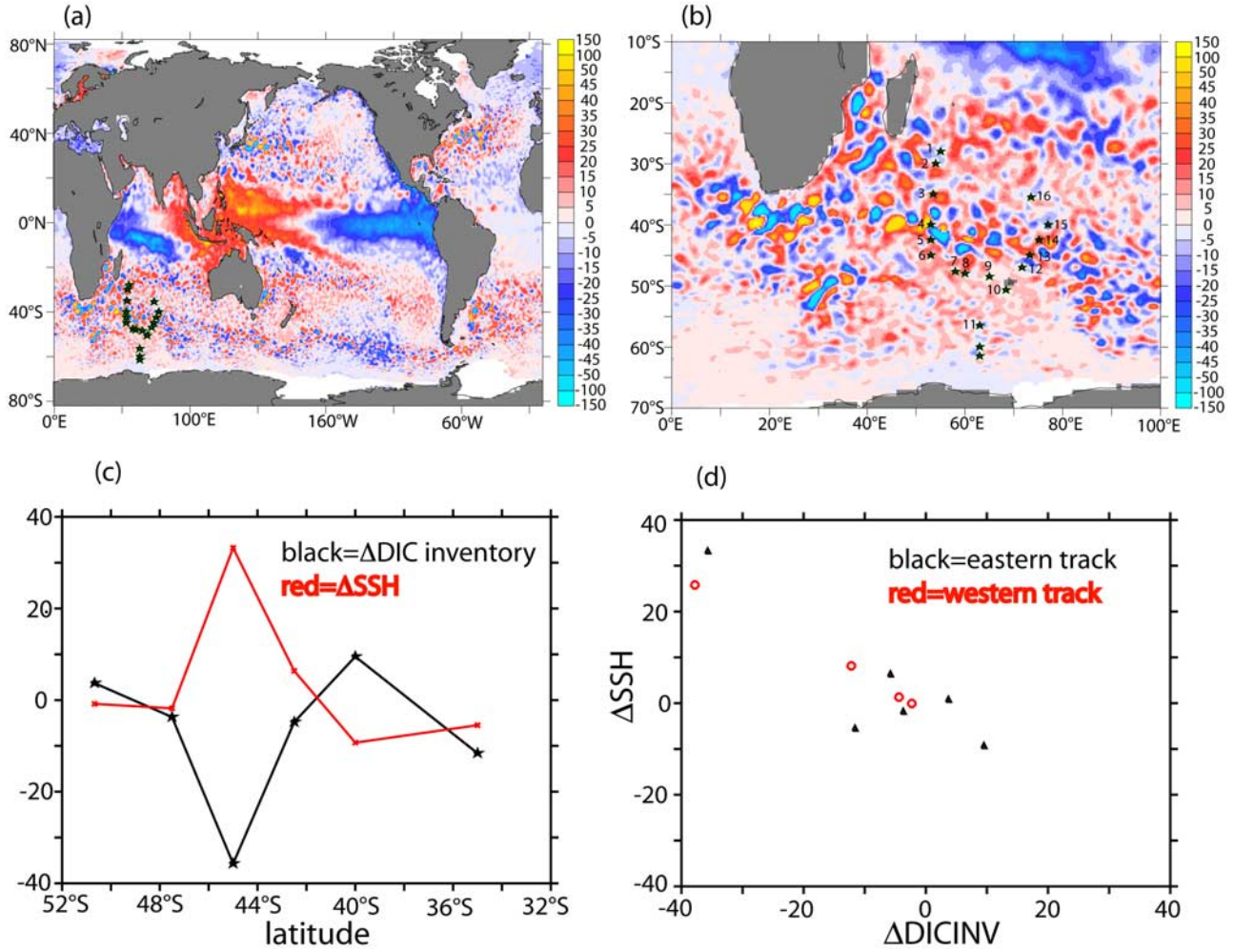

Figure 5. OISO in Southern Indian Ocean; changes between OISO_01 (January 1998) and OISO_03 (December 1998); data from *Jabaud-Jan et al.* [2004] and *Metzl et al.* [2006]. (a) Global changes in SSH from AVISO between January 1998 and December 1998 (cm). (b) Same as Figure 5a, but for the Southern Indian Ocean, with OISO stations overlain as symbols. (c) Changes in DICINV (mol C m^{-2}) and SSH (cm) as a function of latitude. (d) Relationship between ΔDICINV and ΔSSH.

Southern Ocean circulation is also impacted by El Niño through perturbations to the circulation of the extratropical atmosphere. Across the Southern Ocean, there is clearly a zonal structure to the changes over the period, with large mesoscale variability near frontal regions superposed on these changes. For example, in the region bounded by 135°W–110°W, 40°S–70°S in the eastern portion of the Pacific sector, there is an average of a 6.5 cm decrease in SSH between the cruises. For the region bounded by 45°E–85°E, 30°S–70°S, namely the western sector of the Indian Ocean (the sector sampled by OISO), there is a mean increase in SSH of 3.83 cm.

[32] Figure 5b focuses on the changes in SSH in the western Indian Ocean, with (numbered) OISO stations again superposed as symbols. Clearly there are SSH changes spanning a range of spatial scales here. The largest changes are at the mesoscale, and associated with internal variability of the ocean circulation. These are superposed on the smaller-amplitude but larger-scale changes (such as the aforementioned increase of 3.83 cm over 45°E–85°E, 30°S–70°S) that are wind driven and ENSO related. Changes in SSH are explicitly compared with the DIC inventory changes for the stations along the eastern track in Figure 5c. Figure 5c reveals an apparently robust inverse relationship between SSH and DIC inventories.

[33] Changes in SSH (ΔSSH) are plotted against changes in DIC inventories (ΔDICINV) for all of the stations that were sampled during both OISO_01 and OISO_03 in Figure 5d. Figure 5d suggests that a close relationship exists between changes in these variables. For the mean, high (low) SSH and low (high) DICINV are characteristic of the region north (south) of the subpolar front. Clearly the largest changes are due to local changes between waters characteristic of the different sides of the front, through the combined action of mesoscale variations and shifts in the front itself. If the relationship between ΔDICINV and ΔSSH revealed here were to apply to the larger scales, then that would imply that the 3.83 cm averaged changes in SSH for this region would correspond to a decrease of DIC inventories of order 4 mol C m^{-2}. From the data alone it is not possible to answer this question, but we will return to it in our evaluation of model simulations. To the extent that the

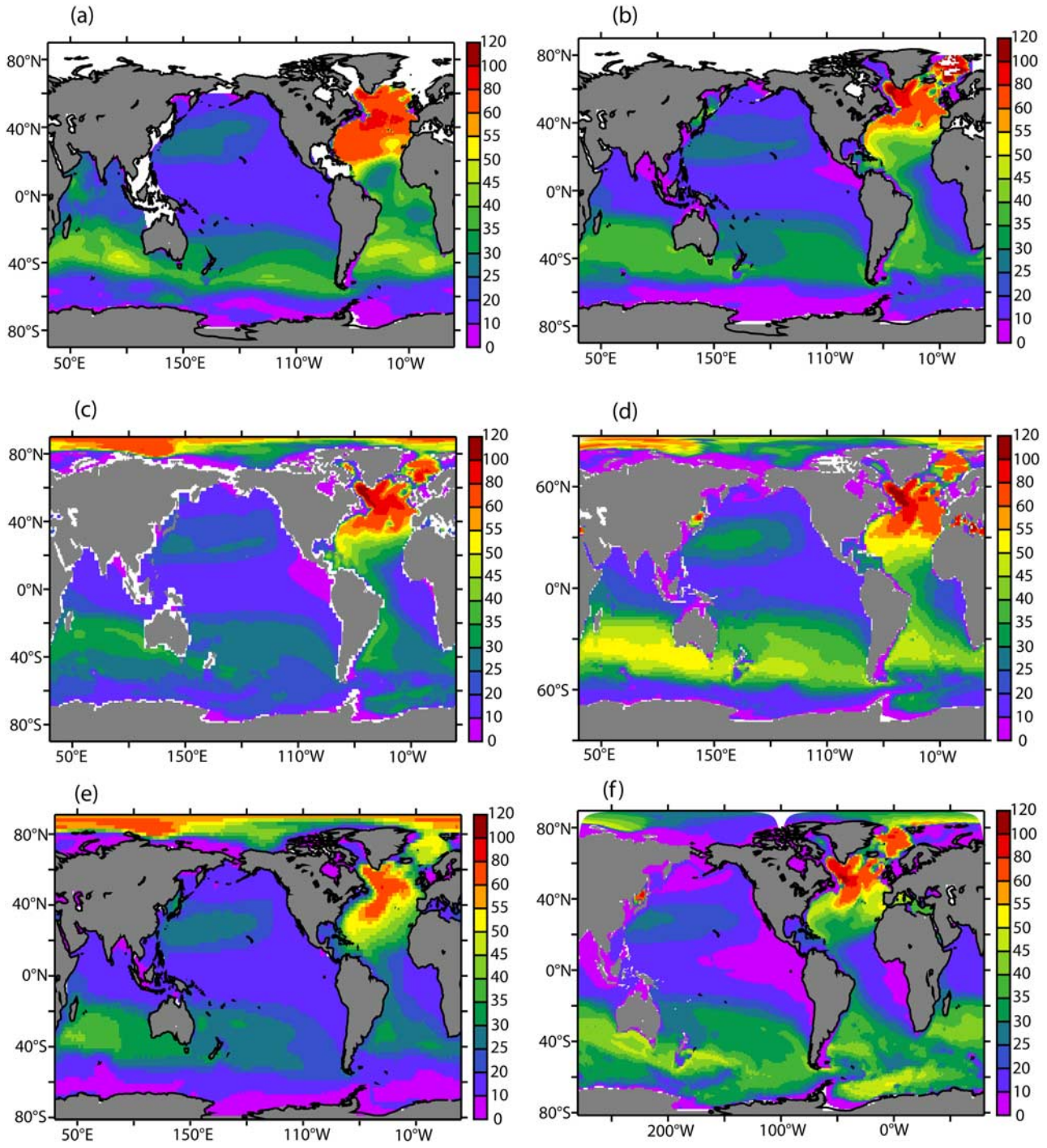

Figure 6. Column inventory of anthropogenic DIC in 1994 (mol C m^{-2}). (a) GLODAP data product, (b) FRCGC model, (c) MPI model, (d) IPSL model, (e) NOAA model, and (f) GFDL model.

relation in Figure 5d does hold on larger scales, it would imply that SSH could help remove biases in extrapolating from local measurements to global inventories.

4.2. Model Results

[34] In order to evaluate whether the changes seen in the observations are representative of larger scales, we turn our attention to three-dimensional model simulations. We first compare the column anthropogenic DIC inventory in 1994 between GLODAP [*Key et al.*, 2004] in Figure 6a and the distributions in the models (Figures 6b–6f). The globally integrated inventory for GLODAP is 118 ± 19 Pg [*Sabine et al.*, 2004], for IPSL is 128.6 Pg, for MPIOM1 is 99.01 Pg, for FRCGC is 101.6 Pg, for NCAR is 96.33 Pg, and for GFDL is 101.9 Pg. The data product has a maximum in the North Atlantic (inventories greater than 60 mol C m^{-2}), and a maximum of significantly larger spatial extent between 20°S–50°S. For the models, the region of maximum

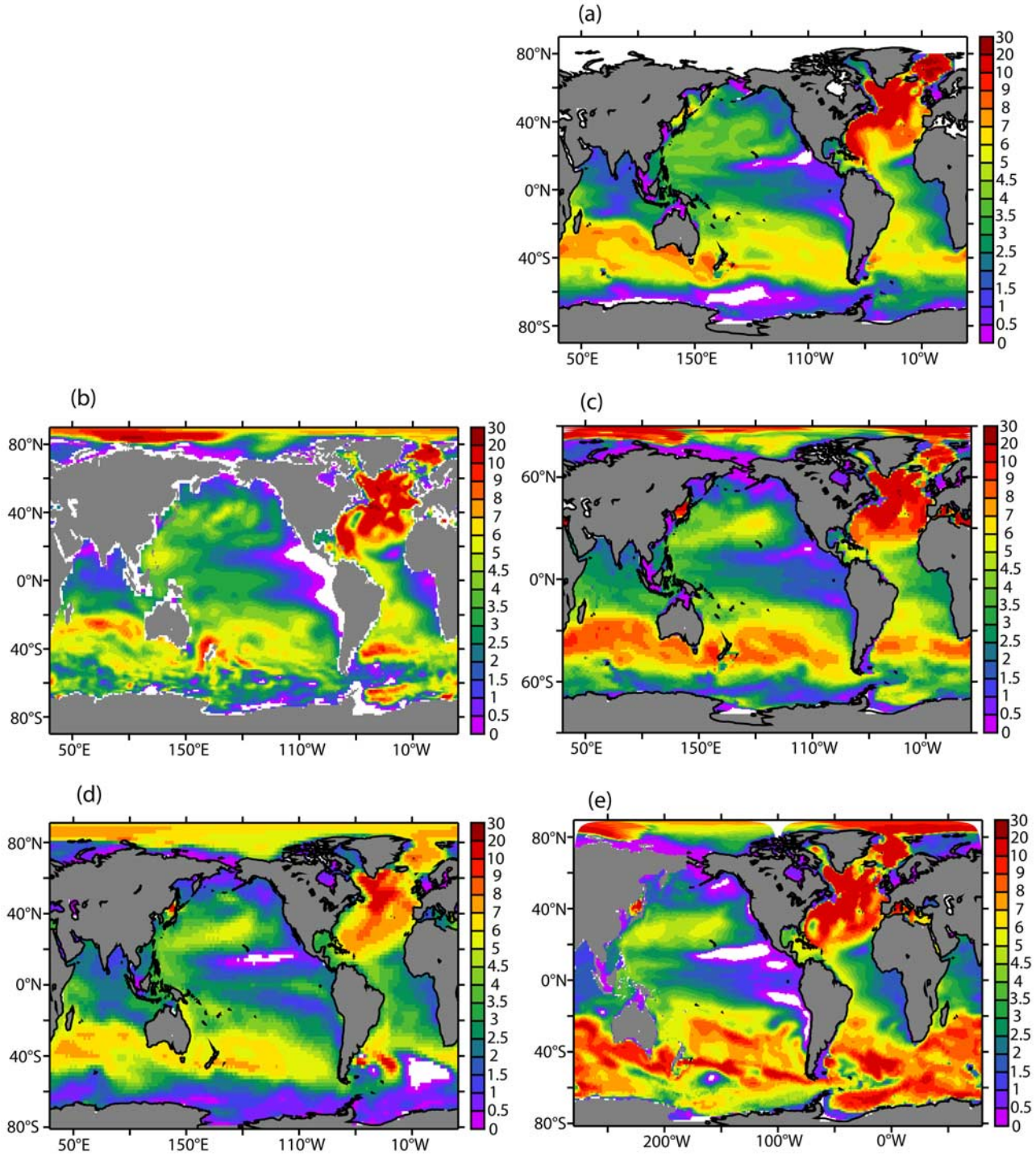

Figure 7. Variations in column inventories of DIC (DICINV) for models (moles C m^{-2}). Changes between May/June 1993 and July/August 2001 for (a) FRCGC, (b) MPI, (c) IPSL, (d) NCAR, and (e) GFDL.

anthropogenic DIC inventories (i.e., with values >60 mol C m^{-2}) has a smaller footprint than in GLODAP, although the models are generally consistent in their representation of the column inventories over the high North Atlantic latitudes. For the North Pacific, the models and GLODAP are internally consistent in that inventories are larger in the subtropical gyre, with specific inventories that are lower than in the North Atlantic. Over the Southern Ocean, inventories are larger between 20°S–50°S, with a tendency to be slightly higher in the Indian Ocean sector than in the Pacific sector.

[35] Next we consider the change in the simulated anthropogenic DIC inventory between 1993 and 2001 for the five models (Figures 7a–7e). The patterns of change are similar to those seen in total WOCE era inventories (Figure 6). The largest changes are found in the North

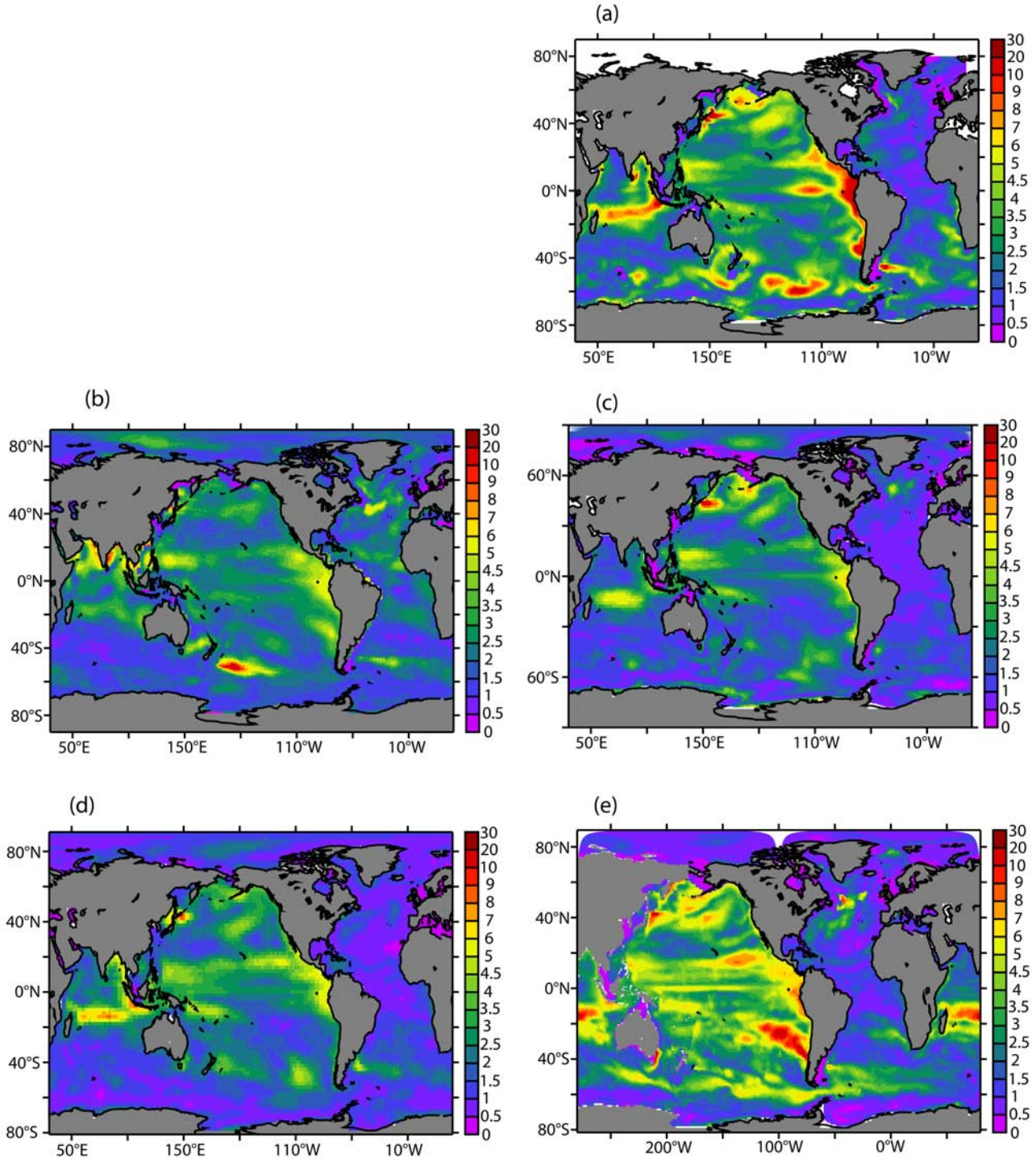

Figure 8. Root mean square of interannually varying detrended monthly anomalies of DIC inventories (mol C m^{-2}) over 1990–2003 for CTL run for (a) FRCGC, (b) MPIOM1, (c) IPSL, (d) NCAR, and (e) GFDL.

Atlantic and the Southern Ocean between 20°S and 50°S. As in Figure 6, there are differences in the simulated distribution, with the inventory increase being largest in GDL and IPSL, and smallest in MPI.

[36] The root mean square of the linearly detrended monthly anomalies of DIC inventories (such that the seasonal cycle has been removed) over 1948–2003 is shown for the CTL simulations in Figures 8a–8e. The structure of the natural variability is similar for the five models, consistent with the results of *Tanhua et al.* [2007], as well as the modeling results of *Levine et al.* [2008]. For some gyre boundary regions the variability exhibits a maximum, and variability is also elevated on the margins or regions where there is a maximum increase in anthropogenic DIC (Figures 7a–7e). Maxima tend to be zonally oriented, and are largest in the models that have the highest horizontal

resolution (FRCGC and GFDL), and lowest in the model that has the lowest horizontal resolution (MPI). For FRCGC and GFDL, with 1° horizontal resolution, it is clear that the amplitude of the natural variability is of the same order as the change in the anthropogenic signal between 1993 and 2001.

[37] The analysis of the observations revealed that changes in DIC inventories on interannual timescales can be closely related to changes in SSH. In order to assess whether these results are representative of the larger scales we turn our attention to one of the models. For this we chose the IPSL model, as among the models considered here this one has received the most extensive model/data comparison for SSH in the study of *Alory et al.* [2005]. The change in SSH between January 1998 and December 1998 (corresponding to the OISO cruises shown in Figure 5) for the ANT simulation with the IPSL model is shown in Figure 9a. Comparison of this simulated ΔSSH field with the ΔSSH from the AVISO data product (Figure 5a) reveals that within the tropics the model captures to first order the large-scale structures of change associated with El Niño. The model also captures changes in the extratropics, for instance with the wind-driven maximum decrease in SSH near 60°S,120°W (Figure 5). Because of its resolution the model does not capture any of the mesoscale variability in the extratropics (even if the model were eddy resolving, it would at best only capture the statistics of eddy-induced variations).

[38] The changes in DIC inventories for the same simulation are shown in Figure 9b. The largest changes are within the tropics, and have a tendency to be anticorrelated with the SSH changes. The changes in the Eastern Equatorial Pacific reflect the shoaling of the thermocline, and the changes under the warm pool in the Western Equatorial Pacific reflect a deepening of the thermocline. In the tropical Indian Ocean, a maximum increase in DIC inventories centered near 10°S is associated with a Rossby wave structure analogous to what was considered for the case of seasonal variability in Figure 3. This structure is also represented in the SSH field (Figure 9a). The correspondence between SSH and DIC inventory changes is also seen in some regions of the extratropics, notably in the Pacific sector of the Southern Ocean.

[39] Figure 9c shows the correlation between detrended monthly anomalies of DIC inventories and SSH over the period 1990–2003, and Figure 9d shows the regression of DICINV anomalies against SSH over the same period. The degree of anticorrelation is elevated throughout the tropics and over most of the subtropics. The anticorrelation is less pronounced poleward of the subantarctic front in the Southern Ocean. The regression map in Figure 9d shows the expected changes in DICINV per cm change in SSH. The two fields are inversely related over most of the global ocean, indicating that the relationships shown in Figures 3 and 4 are representative at larger scales. Interestingly, the absolute amplitude tends to be larger in the Pacific than in the Atlantic, revealing the larger background gradients in DIC found for the Pacific relative to the Atlantic. In the Pacific, the maximum absolute values are found along the margins of the shadow zones in the eastern portion of the basin, again reflecting elevated background gradients in DIC.

[40] The correlation between the detrended monthly anomalies of O2INV and DICINV from ORCA2-PISCES over 1990–2003 are shown in Figure 9e. The fields are anticorrelated over much of the global domain, although there are regions of subtropical and subpolar mode water formation where they become decoupled in both the North Atlantic and the southern oceans. Clearly the pattern here differs somewhat from the correlation between SSH and DICINV shown in Figure 9c. The correlation between detrended monthly anomalies of SSH and O2INV is considered explicitly in Figure 9f. The fields are correlated over much of the tropics, and anticorrelated over large regions of the Southern Ocean and the North Atlantic. The fields are correlated in the eastern part of the North Pacific and anticorrelated in the western reaches of the subtropical gyre.

[41] Finally, we ask how well can anthropogenic DIC inventory changes in the ocean be estimated using the DICINV/SSH regression relationship shown in Figure 9d? The change in anthropogenic DICINV between August 1993 and 2003 for the PRT simulation is shown in Figure 10a, corresponding to the repeat sampling time interval for A16 (20°W) in the North Atlantic. Consistent with what was seen in Figures 6d and 7c for this same model, accumulation tends to be maximum in the North Atlantic and in the Southern Ocean. This represents the target signal of the Repeat Hydrography program. The change in DICINV for the PRT simulation is shown in Figure 10b, and corresponds to what is measured in the ocean.

[42] Next we estimate the anthropogenic DICINV changes using the DICINV changes from the PRT simulation (Figure 10b), the simulated SSH changes over the same time interval (not shown), and the regression relationship between natural DICINV and SSH shown in Figure 9d. The estimated anthropogenic DICINV change is shown in Figure 10c, and the associated error field (Figure 10c minus Figure 10a) is shown in Figure 10d. There are regions where the skill of the estimation is relatively good (the Southern Ocean and the North Atlantic), and regions where the skill is less clear (the North Pacific and the eastern boundary region of the south Pacific subtropical gyre). The RMS of the error in Figure 10d is 3.9 moles C m^{-2}.

[43] The predicted DICINV change obtained using the regression relation between O2INV and DICINV for the CTL simulation is shown in Figure 10e, and the difference between this predicted signal and the explicitly simulated anthropogenic DICINV is shown in Figure 10f. This last panel is the error obtained using an O2INV/DICINV relationship. It is similar to the pattern obtained using SSH/DICINV in some regions and different in others. The RMS of the error for Figure 10f is 3.3 moles C m^{-2}. This reveals that the dynamical information contained in SSH may be of the same order as the biological/physical information contained in the O2INV/DICINV relationship in estimating natural variability in carbon inventories and partitioning natural variability from anthropogenic carbon inventory trends.

5. Discussion

[44] Viewing detection of anthropogenic change as a signal-to-noise problem, the evolving oceanic transient in

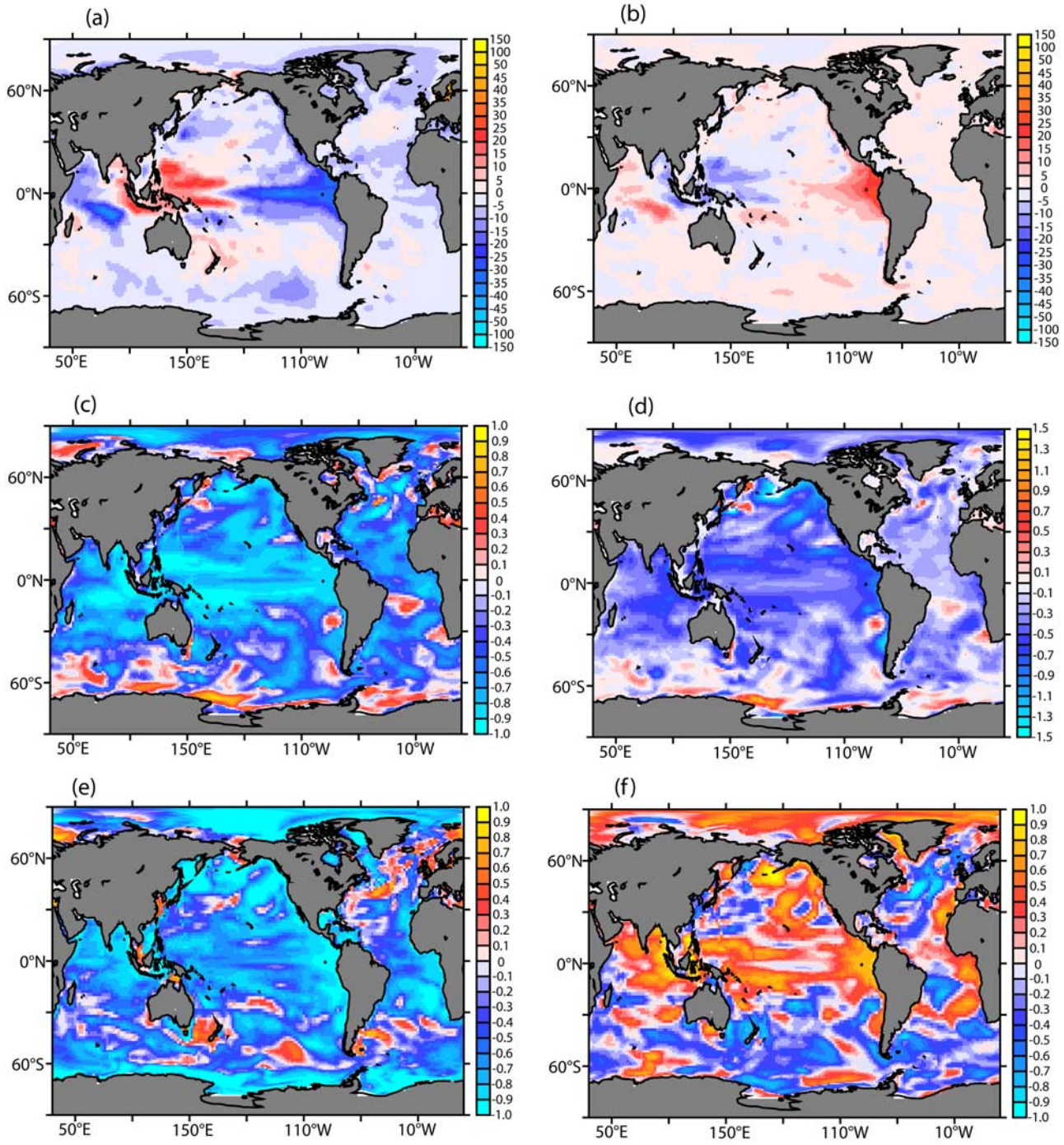

Figure 9. (a) Changes in SSH (ΔSSH, m) for IPSL model between December 1997 and January 1999. (b) Changes in DICINV (mol C m^{-2}) for IPSL model between December 1997 and January 1999. (c) Correlation (point by point) over 1990–2003 of detrended monthly anomalies of SSH and DICINV for IPSL model. (d) Regression (point by point) over 1990–2003 of detrended monthly anomalies of SSH and DICINV for IPSL model. (e) Correlation (point by point) over 1990–2003 of detrended monthly anomalies of O2INV and DICINV for IPSL model. (f) Correlation (point by point) over 1990–2003 of detrended monthly anomalies of O2INV and SSH for IPSL model.

DIC and O_2 must be deconvolved from the background natural variability in DIC and O_2 that has previously been described for both the Pacific [*Sabine et al.*, 2008; *Mecking et al.*, 2008] and the Atlantic [*Johnson and Gruber*, 2007]. *Levine et al.* [2008] argued that an important impediment to reducing uncertainty in carbon detection is our lack of understanding of the processes driving the background variability. This study set out to identify dynamically driven changes in ocean DIC and O_2 measurements by linking measured changes in these fields to changes in the physical state of the ocean. As the number of repeat DIC measurements is relatively small, models were used to consider

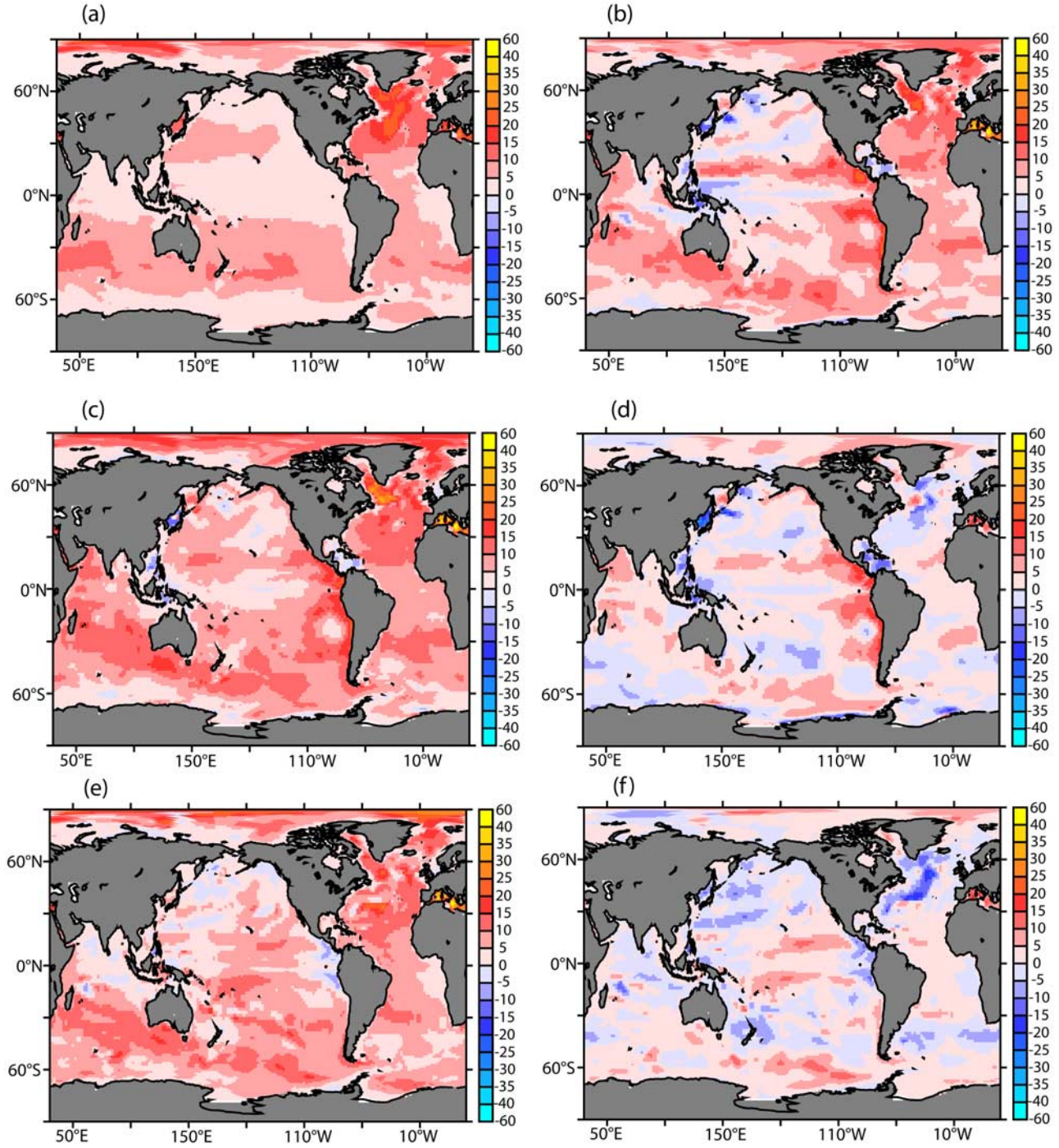

Figure 10. (a) Change in anthropogenic DICINV (PRT-CTL, mol C m^{-2}) between August 1993 and 2003. (b) Changes in DICINV (mol C m^{-2}) for PRT simulation between August 1993 and 2003. (c) Estimated anthropogenic DICINV change (mol C m^{-2}) between August 1993 and 2003 using simulated SSH to correct DICINV from PRT simulation. (d) Error in estimate of DICINV (Figure 10c minus Figure 10a, mol C m^{-2}). (e) Estimated anthropogenic DICINV change (mol C m^{-2}) between August 1993 and 2003 using simulated O2INV to correct DICINV from PRT simulation. (f) Error in estimate of anthropogenic DICINV (Figure 10e minus Figure 10a, mol C m^{-2}).

whether the relationships identified in the data are representative over larger scales.

[45] For the Indian Ocean section shown in Figure 3d, the high correspondence between changes in SSH, DIC inventories, and O_2 inventories supports our hypothesis that the convergence term in equation (2) makes a first-order contribution to the background natural variability of DIC and O_2. Our hypothesis is also consistent with the changes seen for OVIDE in the North Atlantic (Figure 4). There we argued that a decoupling of DIC and O_2 inventory changes

over a 2-year period is a consequence of differences in the mean state for the two fields (namely that $\nabla\overline{O_2}$ is large and it is small for $\nabla\overline{DIC}$). If one were to argue that the changes in both DICINV and O2INV for I8N (Figure 3) and the changes in O2INV for OVIDE (Figure 4) were due to nonlocal changes in ventilation processes, then one would need to explain as a coincidence that the tracer inventory changes corresponding to dynamical changes (themselves manifested in SSH changes). It is worth reiterating that these changes are associated with seasonal Rossby wave perturbations in the Indian Ocean, and thus they occur independently of any of the major climate modes (ENSO etc.).

[46] In asserting first-order importance for the transport term in equation (2) as a first-order driver of variability in upper ocean DIC, it is not our intention to imply that other processes described in the Introduction (biology, gas exchange ventilation, and mesoscale variability) are not important. *Levine et al.* [2008] have argued that variability in ventilation processes in their model drives a decoupling of DIC and O_2 near subpolar frontal regions. *Deutsch et al.* [2006] emphasized that both the transport and convergence terms of equation (2) are likely to contribute to decadal variability in thermocline O_2 concentrations for the North Pacific. Our analysis does not contradict their main results. We emphasize that the convergence term is also important, and that for many cases it can be detected with altimetry. Importantly, processes such as gas exchange and biology play critical supporting roles for this type of variability in maintaining mean background gradients in tracer concentrations.

[47] As yet there is little in the way of a general descriptive account in the climate literature of the dominant structures and timescales of variability of DIC and O_2 in the global ocean. For the physical state of the climate system, the studies of *Hasselmann* [1976] and *Frankignoul and Hasselmann* [1977] argued using theoretical considerations and simplified models that variability in ocean circulation should be expected on all timescales. To date there is very little (if any) indication that there is a significant spectral peak for variations in the physical state of the ocean. It is important to keep this in mind when interpreting decadal repeat measurements collected with an Eulerian detection network consisting largely of long ocean transects. With such a sampling higher frequency (seasonal to interannual) variations will be aliased into the measurements. As Rossby waves are a source of background variability in DIC and O_2 distributions, we emphasize that satellite-derived SSH changes can help deconvolve natural and anthropogenic changes in DIC and O_2. Altimetry measurements are available at high spatial and temporal resolution for 1992 to present. This spans many of the WOCE transects and all of the CLIVAR transects. The development of a new method for incorporating this dynamical information into the eMLR-type [*Friis et al.*, 2005] detection methods is currently being pursued as a separate project, building on the implications of the present study.

[48] Regarding spatial patterns of variability, our analysis of the structures of natural variability in DIC inventories on seasonal to interannual timescales reveals that the characteristic global patterns are different form the pattern assumed by the anthropogenic transient. This is consistent with the interpretation of c4oupled model output presented in the study of *Levine et al.* [2008], where the focus was primarily on changes along a particular transect (A16 in the Atlantic). Whereas the anthropogenic inventories tend to be large in well-ventilated regions, the natural variability tends to be largest in regions that are associated with large background gradients in tracer quantities that coincide with large gradients in hydrographic properties.

[49] There are two final caveats that are important to the application of the SSH/DIC inventory relation emphasized here to the problem of detection of anthropogenic DIC in the ocean. First, our analysis did not account for mesoscale variations. As has been shown by *McGillicuddy et al.* [1999], not all mesoscale variability will have the same SSH to thermocline depth relationship. Thus it will be important in future work to identify whether the relationships considered here between SSH and DIC inventories hold for mesoscale variations.

[50] The second caveat involves the seasonal cycle. Importantly, the "test of concept" presented in Figure 10 relied on model fields from which seasonal variations had been removed through filtering. Specifically, the calculations involved (detrended) monthly anomalies. Thus our assertion of the utility of the SSH/DIC inventory relation must be understood within this context. For practical reasons Repeat Hydrography sampling will not be able to resample select transects during the identical month with decadal repeats. Thus is will be important to address quantitatively the relationship between SSH and DIC inventories over seasonal timescales. In recognition of the importance of this question, two of the coauthors of the present study (Chris Winn and Keith Rodgers) have begun work on a separate process study focusing on the seasonal cycle for stations that fully resolve the seasonal cycle (beginning with Ocean Station ALOHA).

6. Conclusions

[51] Our main finding is that convergence and divergence (column stretching) associated with Rossby wave activity can provide a first-order contribution to the background variability in column inventories of DIC and O_2 in the ocean. We began by testing this with available short-timescale (6–24 month) repeat measurements of ocean biogeochemistry. The importance of Rossby waves was revealed most clearly in the tropical Indian Ocean (Figure 3), where the scales of the respective perturbations were unambiguously larger than those of mesoscale eddies. Models were subsequently used to argue that the relationships identified in the relatively sparse short-timescale measurements are representative over larger scales. Importantly, the analyses illustrated that the natural variations in DIC are often well correlated with changes in sea surface height (SSH).

[52] We hope that the results presented here will stimulate development of new methods to detect anthropogenic DIC accumulation in the ocean. For detection, the background variability is noise. Therefore satellite-derived SSH data products should help deconvolve the anthropogenic and natural variability components of the measured DIC changes. Specifically, including dynamical information can complement detection algorithms of the type presented

in the studies of *Friis et al.* [2005] and *Levine et al.* [2008] and help to reduce uncertainty. Additionally it will be important to explicitly test the extent to which the effects of eddies on tracers through layer convergence/divergence correspond to changes in SSH as well.

Appendix A: Description of Models

[53] Results from all five of the models presented here were generated using biogeochemical models imbedded (online) in three-dimensional physical circulation models of the global ocean. These models collectively represent the next step forward from the generation of models used during the OCMIP-2 (http://www.ipsl.jussieu.fr/OCMIP/phase2) project, with each model thereby following the protocols of the European North Ocean Carbon Exchange Study (NOCES) project (http://www.ipsl.jussieu.fr/OCMIP/phase3/), or OCMIP-3. The important features shared by each of the five models considered here are as follows:

[54] 1. The models are forced with interannually varying surface momentum and buoyancy fluxes. Thus the surface boundary conditions contain variations associated with El Nino etc. Three of the models are forced at the surface with NCEP-1 reanalysis fluxes, one is forced with NCEP-2, and one is forced with CORE fluxes (themselves NCEP-derived).

[55] 2. All of the models feature fully prognostic biogeochemistry models. As such, there is no restoring of nutrient fields to observed values at the sea surface.

[56] 3. A free surface formulation is now a common feature of the dynamical formulation of the models, with this feature allowing for the conservation of salt in the ocean interior. Thus the spurious ''virtual fluxes'' of properties that was characteristic of the OCMIP-2 generation of models is no longer present.

[57] For each model two separate runs were performed, a steady state CO_2 run and a transient run. The runs differ in their atmospheric boundary conditions used for CO_2 concentrations. The first uses the atmospheric transient over 1760–2002 (the PRT or perturbation simulation), and the second (the CTL or control simulation) uses constant preanthropogenic concentrations of 278 μatm. For the historical boundary condition for atmospheric CO_2, a cubic spline fit has been applied to the Law Dome ice core data of *Etheridge et al.* [1996] and the Mauna Loa atmospheric CO_2 observations [*Enting et al.*, 1994]. The record has been extended past 1990 with a 12-month running mean of the Mauna Loa CO_2 record.

[58] The differences between the various models are highlighted below. Importantly, the models have followed different methods for initialization and spin-up, and these details are included in the descriptions of the various models. Additionally, some of the models used different reanalysis or reanalysis-derived products for their surface boundary conditions. Three of the models have used NCEP-1 reanalysis fluxes [*Kalnay et al.*, 1996], one has used NCEP-2 reanalysis fluxes [*Kalnay et al.*, 1996], and one model has used fluxes from the Coordinated Ocean-Ice Reference Experiment (CORE) project [*Large and Yeager*, 2004; *Griffies et al.*, 2009].

A1. ORCA2-PISCES (the "IPSL" Simulation)

[59] ORCA2-PISCES is the ORCA2 ocean model [*Madec et al.*, 1999] and the PISCES biogeochemistry model [*Aumont and Bopp*, 2006], and was previously analyzed in the studies of *Raynaud et al.* [2005] and *Rodgers et al.* [2008a, 2008b]. The runs use the forcing configurations presented by *Rodgers et al.* [2004]. The surface forcing for the historical period is NCEP-1 [*Kalnay et al.*, 1996] fluxes, with surface heat fluxes calculated using bulk formulas.

[60] The physical circulation model took initial conditions for temperature and salinity from the climatologies of *Boyer et al.* [1998] and *Antonov et al.* [1998], respectively. From this initial state, the ocean model was spun up through two cycles of NCEP-1 over 1948–2003 for a total of 112 years. A restoring timescale for surface salinity of 12 days is applied for the 10-m-thick surface layer to the climatology of *Boyer et al.* [1998]. The spin-up with the PISCES biogeochemistry model was performed separately for 5000 years with circulation fields taken from monthly climatological circulation fields, after initializing with GLODAP [*Key et al.*, 2004] and World Ocean Atlas 2001 [*Conkright et al.*, 2002a, 2002b] nutrient fields. Over the period 1765–1947, two separate simulations were performed offline with PISCES of which one maintained constant atmospheric CO_2 and one included the anthropogenic transient. For the component of the simulations presented here, the initial states for the dynamical and biogeochemical models were taken for initialization on 1 January 1948 from these spin-ups, and the model simulations analyzed here span 1948–2003.

A2. MPIOM-HAMOCC5 (the "MPI" Simulation)

[61] MPIOM-HAMOCC5 is the MPI ocean model (MPI-OM) [*Marsland et al.*, 2003] and the Hamburg oceanic carbon cycle model HAMOCC5, and was presented in the study of *Wetzel et al.* [2005]. This model was also forced with NCEP-1 reanalysis fluxes, and bulk formulas were used to calculate surface buoyancy fluxes. The model maintained a time constant of 180 days for restoring salinity in the top 12-m layer to the climatology of *Boyer et al.* [1998].

[62] The ocean model was initialized with annual mean temperature and salinity from the climatology of *Antonov et al.* [1998] and *Boyer et al.* [1998]. The biogeochemical model was started with a uniform tracer distribution, and during the first year of integration the three-dimensional temperature and salinity distributions were restored to the *Antonov et al.* [1998] and *Boyer et al.* [1998] climatologies with a time constant of 180 days. After initialization of the model, it was integrated by periodically repeating the forcing with a linearly detrended set of the NCEP-1 fields from 1948 to 2001 for a total of 2700 model years. At this point the fluxes and tracer distributions had become cyclostationary and a preindustrial CO_2 level of 278 μatm was matched.

[63] From this preindustrial state the main experiments ran over 1765–2003 (one run with continued preanthropogenic CO_2 concentrations and the other with the transient). From the year 1948 on, the original NCEP-1 fields with their inherent trends were used to force the model.

A3. COCO-NEMURO (the "FRCGC" Simulation)

[64] COCO-NEMURO is the CCSR Ocean Component Model (COCO) and the North Pacific Ecosystem Model Used for Regional Oceanography (NEMURO) [*Aita et al.*, 2003; *Yamanaka et al.*, 2004]. The model is forced with NCEP-1 reanalysis fluxes. For temperature, the direct sea surface heat fluxes from NCEP are applied to the model, with no restoring boundary condition for temperature. Surface salinity was restored to the climatology of *Levitus and Boyer* [1994] with a timescale of 100 days.

[65] The ocean model was initialized using he climatologies for salinity and temperature of *Levitus et al.* [1994]. The model was run for several thousand years until a quasi-equilibrium state was achieved [*Nakano*, 2000]. The ocean biogeochemistry fields were initialized using the nutrient climatologies of *Conkright et al.* [1994] for NO_3 and Si, and GLODAP [*Key et al.*, 2004] for DIC. The COCO-NEMURO run was then spun up for four cycles using daily averaged surface buoyancy fluxes for a total of 220 years.

A4. CCSM3-BEC (the "NCAR" Simulation)

[66] CCSM3-BEC is the Community Climate System Model ocean Biogeochemical Element Cycle model [*Doney et al.*, 2009a, 2009b]. This model was forced with NCEP-2 reanalysis fluxes, and surface buoyancy fluxes were calculated using bulk formulas. Surface salinity was restored to observations through a restoring of 0.0115 g/m2/s/psu.

[67] The model was initialized with the preindustrial DIC distribution of GLODAP [*Key et al.*, 2004], and initial conditions for temperature and salinity were taken from the World Ocean Atlas data. The model was first run for 600 years with a repeating annual cycle of forcing and preindustrial atmospheric CO_2 (278 μatm) to get the air-sea fluxes as close as possible to equilibrium. Then at model year 601 (1765) the control run branched into two runs, one with preindustrial boundary conditions and the other with the anthropogenic transient in atmospheric CO_2 concentrations. The hindcast runs presented here have branched off this anthropogenic CO_2 run in years 1958 and 1979.

A5. MOM4-TOPAZ (the "GFDL" Simulation)

[68] MOM4-TOPAZ is the Modular Ocean Model Version 4 (MOM4) [*Griffies et al.*, 2003, 2005; *Gnanadesikan et al.*, 2006] and GFDL's Tracers for Ocean Phytoplankton with Allometric Zooplankton (TOPAZ) [*Dunne et al.*, 2008]. This model was forced with the NCEP derived CORE fields over 1959–2004 [*Large and Yeager*, 2004; *Griffies et al.*, 2009]. Surface salinity was restored to observations with a 60 day timescale for the upper 10 m layer. The model version analyzed here is the same as that described in the study of *Henson et al.* [2009].

[69] The model was initialized with World Ocean Atlas 2001 temperature [*Stephens et al.*, 2002], salinity [*Boyer et al.*, 2002], and nutrient data [*Conkright et al.*, 2002a, 2002b] and GLODAP [*Key et al.*, 2004] DIC data, and then spun up for two cycles of CORE forcing over 1959–2004 with preindustrial boundary conditions. The starting in the third cycle (in 1785) the model was split into two branches, one with preindustrial and one with transient atmospheric CO_2 boundary conditions. Both cases were iterated for an additional 5 loops, with the 5th loop corresponding to the years 1959–2004.

[70] **Acknowledgments.** Special thanks are due to Stephanie Henson for her insights and suggestions regarding the AVISO data product and to Sara Mikaloff Fletcher for her constructive criticisms with the original manuscript. This report was prepared by K.B.R. under awards NA17RJ2612 and NA08OAR4320752, which includes support through the NOAA Office of Climate Observations (OCO). The statements, findings, conclusions, and recommendations are those of the authors and do not necessarily reflect the views of the National Oceanic and Atmospheric Administration or the U.S. Department of Commerce. Support for K.B.R. was also provided by the Carbon Mitigation Initiative (CMI) through the support of BP, Amaco, and Ford. R.M.K. was supported by NOAA grants NA17RJ2612, NA08OAR4320752, and NA08OAR4310820. F.F.P. was supported by the European Union FP6 CARBOOCEAN Integrated project (contract 51176), the French OVIDE project, and the Spanish Salvador de Madariaga program (PR2006–0523). This work was also supported by the European NOCES project (EVK2-CT201-00134). Y.Y. and A.I. are partly supported by CREST, JST of Japan. The long-term OISO observational program in the South Indian Ocean is supported by the following three French institutes: INSU (Institut National des Sciences de l'Univers), IPSL (Institute Pierre-Simon Laplace), and IPEV (Institut Paul-Emile Victor).

References

Aita, M. N., Y. Yamanaka, and M. J. Kishi (2003), Effects of ontogenetic vertical migration of zooplankton on annual primary production using NEMURO embedded in a general circulation model, *Fish. Oceanogr.*, *12*, 284–290, doi:10.1046/j.1365-2419.2003.00261.x.

Alory, G., S. Cravatte, T. Izumo, and K. B. Rodgers (2005), Validation of a decadal OGCM simulation for the tropical Pacific, *Ocean Modell.*, *10*(3–4), 272–282.

Antonov, J., S. Levitus, T. P. Boyer, M. Conkright, T. O'Brien, and C. Stephens (1998), *World Ocean Atlas 1998*, vol. 2, *Temperature of the Pacific Ocean*, *NOAA Atlas NESDIS*, vol. 28, 166 pp., NOAA, Silver Spring, Md.

Antonov, J. I., R. A. Locarnini, T. P. Boyer, A. V. Mishonov, and H. E. Garcia (2006), *World Ocean Atlas 2005*, vol. 2, *Salinity*, *NOAA Atlas NESDIS*, vol. 62, 182 pp., NOAA, Silver Spring, Md.

Aumont, O., and L. Bopp (2006), Globalizing results from ocean in situ iron fertilization studies, *Global Biogeochem. Cycles*, *20*, GB2017, doi:10.1029/2005GB002591.

Bender, M., et al. (2002), *A Large-Scale CO^2 Observing Plan: In Situ Oceans and Atmosphere*, U.S. Dep. of Commer., Washington, D. C.

Boyer, T. P., S. Levitus, J. Antonov, M. Conkright, T. O'Brien, and C. Stephens (1998), *World Ocean Atlas 1998*, vol. 5, *Salinity of the Pacific Ocean*, *NOAA Atlas NESDIS*, vol. 31, 166 pp., NOAA, Silver Spring, Md.

Boyer, T. P., C. Stephens, J. I. Antonov, M. E. Conkright, R. A. Locarnini, T. D. O'Brien, and H. E. Garcia (2002), *World Ocean Atlas 2001* [CD-ROM], vol. 2, *Salinity*, *NOAA Atlas NESDIS*, vol. 50, 165 pp., NOAA, Silver Spring, Md.

Conkright, M. E., S. Levitus, and T. P. Boyer (1994), *World Ocean Atlas 1994*, vol. 1, *Nutrient*, *NOAA Atlas NESDIS*, vol. 1, 162 pp., NOAA, Silver Spring, Md.

Conkright, M. E., H. E. Garcia, T. D. O'Brien, R. A. Locarnini, T. P. Boyer, C. Stephens, and J. I. Antonov (2002a), *World Ocean Atlas 2001* [CD-ROM], vol. 4, *Nutrients*, *NOAA Atlas NESDIS*, vol. 52, 392 pp., NOAA, Silver Spring, Md.

Conkright, M. E., R. A. Locarnini, H. E. Garcia, T. D. O'Brien, T. P. Boyer, C. Stephens, and J. I. Antonov (2002b), World ocean atlas 2001: Objective analyses, data statistics, and figures [CD-ROM], *Internal Rep. 17*, Natl. Oceanogr. Data Cent., Silver Spring, Md.

Deutsch, C., S. Emerson, and L. Thompson (2005), Fingerprints of climate change in North Pacific Oxygen, *Geophys. Res. Lett.*, *32*, L16604, doi:10.1029/2005GL023190.

Deutsch, C., S. Emerson, and L. Thompson (2006), Physical-biological interactions in the North Pacific oxygen variability, *J. Geophys. Res.*, *111*, C09S90, doi:10.1029/2005JC003179.

Doney, S. C., S. Yeager, G. Danabasoglu, W. G. Large, and J. C. McWilliams (2007), Mechanisms governing interannual variability of upper ocean temperature in a global hindcast simulation, *J. Phys. Oceanogr.*, *37*, 1918–1938, doi:10.1175/JPO3089.1.

Doney, S. C., I. Lima, R. A. Feely, D. M. Glover, K. Lindsay, N. Mahowald, J. K. Moore, and R. Wanninkhof (2009a), Mechanisms governing interannual variability in the upper-ocean inorganic carbon system and air-sea CO_2 fluxes: Physical climate and atmospheric dust, *Deep Sea Res. Part II*, *56*, 640–655.

Doney, S. C., I. Lima, J. K. Moore, K. Lindsay, M. Behrenfeld, T. K. Westberry, N. Mahowald, D. M. Glover, and T. Takahashi (2009b), Skill metrics for confronting global upper ocean ecosystem-biogeochemistry models against field and remote sensing data, *J. Mar. Systems*, *76*(1–2), 95–112.

Dunne, J. P., A. Gnanadesikan, and J. L. Sarmiento (2008), Coupling between the C, N, Fe, P., Si, Ca, and lithogenic cycles in a global ocean biogeochemical and ecological model, paper presented at 2008 Ocean Sciences Meeting, Am. Soc. of Limnol. and Oceanogr., Orlando, Fla.

Emerson, S., Y. W. Watanabe, T. Ono, and S. Mecking (2004), Temporal trends in apparent oxygen utilization in the upper pycnocline of the North Pacific: 1980–2000, *J. Oceanogr.*, *60*, 139–147, doi:10.1023/B:JOCE.0000038323.62130.a0.

Enting, I. G., T. M. L. Wigley, and M. Heimmann (1994), Future emissionas and concentrations of carbon dioxide: Key ocean/atmosphere/land analyses, *Tech. Pap. 31*, Commonw. Sci. and Ind. Res. Organ., Clayton South, Victoria, Australia.

Etheridge, D. M., L. P. Seele, R. L. Langefelds, R. J. Francey, J.-M. Barnola, and V. I. Morgan (1996), Natural and anthropogenic changes in atmospheric CO_2 over the last 100 years from air in Antarctic ice and firn, *J. Geophys. Res.*, *101*, 4115–4128, doi:10.1029/95JD03410.

Frankignoul, C., and K. Hasselmann (1977), Stochastic climate models. Part II. Application to SST anomalies and thermocline variability, *Tellus*, *29*, 289–305.

Friis, K., A. Kortzinger, J. Patch, and D. W. R. Wallace (2005), On the temporal increase of anthropogenic CO_2 in the subpolar North Atlantic, *Deep Sea Res. Part I*, *52*, 681–698, doi:10.1016/j.dsr.2004.11.017.

Garcia, H. E., R. A. Locarnini, T. P. Boyer, and J. I. Antonov (2006), *World Ocean Atlas 2005*, vol. 2, *Oxygen, Apparent Oxygen Utilization, and Oxygen Saturation*, *NOAA Atlas NESDIS*, vol. 63, 342 pp., NOAA, Silver Spring, Md.

Gnanadesikan, A., et al. (2006), GFDL's CM2 global coupled climate models. Part II: The baseline ocean simulation, *J. Clim.*, *19*(5), 675–697, doi:10.1175/JCLI3630.1.

Griffies, S. M., M. J. Harrison, R. C. Pacanowski, and A. Rosati (2003), A technical guide to MOM4, *Geophys. Fluid Dyn. Lab. Ocean Group Tech. Rep. 5*, 295 pp., NOAA, Princeton, N. J.

Griffies, S. M., et al. (2005), Formulation of an ocean model for global climate simulations, *Ocean Sci.*, *1*, 45–79.

Griffies, S. M., et al. (2009), Coordinated ocean-ice reference experiments (CORE s), *Ocean Modell.*, *26*(1–2), 1–46, doi:10.1016/j.ocemod.2008.08.007.

Hasselmann, K. (1976), Stochastic climate models. Part I. Theory, *Tellus*, *28*, 463–485.

Henson, S. A., J. P. Dunne, and J. L. Sarmiento (2009), Decadal variability in North Atlantic phytoplankton blooms, *J. Geophys. Res.*, *114*, C04013, doi:10.1029/2008JC005139.

Jabaud-Jan, A., N. Metzl, C. Brunet, A. Poisson, and B. Schauer (2004), Variability of the carbon dioxide system in the southern Indian Ocean (20°S–60°S): The impact of a warm anomaly in austral summer 1998, *Global Biogeochem. Cycles*, *18*, GB1042, doi:10.1029/2002GB002017.

Johnson, G. C., and N. Gruber (2007), Decadal water mass variations along 20°W in the Northeastern Atlantic Ocean, *Prog. Oceanogr.*, *73*(304), 277–295.

Johnson, K. M., et al. (1998), Coulometric total carbon dioxide analysis for marine studies: An assessment of the quality of total inorganic carbon measurements made during the US Indian Ocean CO_2 survey 1994–1996, *Mar. Chem.*, *63*, 21–37, doi:10.1016/S0304-4203(98)00048-6.

Kalnay, E. C., et al. (1996), The NCEP/NCAR reanalysis project, *Bull. Am. Meteorol. Soc.*, *77*, 437–471, doi:10.1175/1520-0477(1996)077<0437:TNYRP>2.0.CO;2.

Key, R. M., A. Kozyr, C. L. Sabine, K. Lee, R. Wanninkhof, J. L. Bullister, R. A. Feely, F. J. Millero, C. Mordy, and T.-H. Peng (2004), A global ocean carbon climatology: Results from Global Ocean Data Analysis Project (GLODAP), *Global Biogeochem. Cycles*, *18*, GB4031, doi:10.1029/2004GB002247.

Large, W., and S. Yeager (2004), Diurnal to decadal global forcing for ocean and sea ice models: the data sets and flux climatologies, *Tech. Note NCAR/TN-460+STR*, Natl. Cent. for Atmos. Res., Boulder, Colo.

Le Traon, P. Y., Y. Faugere, F. Hernandez, J. Dorandeu, F. Mertz, and M. Ablain (2003), Can we merge GEOSAT follow-on with TOPEX/Poseidon and ERS-2 for an improved description of the ocean circulation?, *J. Atmos. Oceanic Technol.*, *20*(6), 889–895, doi:10.1175/1520-0426(2003)020<0889:CWMGFW>2.0.CO;2.

Levine, N. M., S. C. Doney, R. Wanninkhof, K. Lindsay, and I. Y. Fung (2008), The impact of ocean carbon system variability on the detection of temporal increases in anthropogenic CO_2, *J. Geophys. Res.*, *113*, C03019, doi:10.1029/2007JC004153.

Levitus, S., and T. P. Boyer (1994), *World Ocean Atlas 1994*, vol. 4, *Temperature*, *NOAA Atlas NESDIS*, vol. 4, 129 pp., NOAA, Silver Spring, Md.

Levitus, S., R. Burgett, and T. P. Boyer (1994), *World Ocean Atlas 194*, vol. 3, *Salinity*, *NOAA Atlas NESDIS*, vol. 3, 111 pp., NOAA, Silver Spring, Md.

Lherminier, P., H. Mercier, C. Gourcuff, M. Alvarez, S. Bacon, and C. Kermabon (2007), Transports across the 2002 Greenland-Portugal Ovide section and comparison with 1997, *J. Geophys. Res.*, *112*, C07003, doi:10.1029/2006JC003716.

Locarnini, R. A., A. V. Mishonov, J. I. Antonov, T. P. Boyer, and H. E. Garcia (2006), *World Ocean Atlas 2005*, vol. 1, *Temperature*, *NOAA Atlas NESDIS*, vol. 61, 182 pp., NOAA, Silver Spring, Md.

Madec, G., P. Delecluse, M. Imbard, and C. Levy (1999), *OPA 8.1 Ocean General Circulation Model Reference Manual*, Lab. d'Océanogr. Dyn. et de Climatol., Paris.

Marsland, S. J., H. Haak, J. H. Jungclaus, M. Latif, and F. Roeske (2003), The Max-Planck-Institute global ocean/sea ice model with orthogonal curvilinear coordinates, *Ocean Modell.*, *5*, 91–127, doi:10.1016/S1463-5003(02)00015-X.

McGillicuddy, D. J., Jr., R. Johnson, D. A. Siegel, A. F. Michaels, N. R. Bats, and A. H. Knap (1999), Mesoscale variations of biogeochemical properties in the Sargasso Sea, *J. Geophys. Res.*, *104*, 13,381–13,394, doi:10.1029/1999JC900021.

McPhaden, M. J., and D. Zhang (2004), Pacific Ocean circulation rebounds, *Geophys. Res. Lett.*, *31*, L18301, doi:10.1029/2004GL020727.

Mecking, S., C. Langdon, R. A. Feely, C. L. Sabine, C. A. Deutsch, and D.-H. Min (2008), Climate variability in the North Pacific thermocline diagnosed from oxygen measurements: An update based on the U.S. CLIVAR/CO_2 Repeat Hydrography cruises, *Global Biogeochem. Cycles*, *22*, GB3015, doi:10.1029/2007GB003101.

Metzl, N., C. Brunet, A. Jabaud-Jan, A. Poisson, and B. Schauer (2006), Summer and winter air-sea CO_2 fluxes in the Southern Ocean, *Deep Sea Res. Part I*, *53*, 1548–1563, doi:10.1016/j.dsr.2006.07.006.

Nakano, H. (2000), Modeling global abyssal circulation by incorporating bottom boundary layer parameterization, Ph.D. thesis, 110 pp., Univ. of Tokyo, Tokyo.

Pascual, A., Y. Faugere, G. Larnicol, and P. Y. Le Traon (2006), Improved description of the ocean mesoscale variability by combining four satellite altimeters, *Geophys. Res. Lett.*, *33*, L02611, doi:10.1029/2005GL024633.

Peltola, E., et al. (1998), Chemical and hydrographic measurements during the Indian Ocean I8 repeat cruise (I8N) during September and October, 1995, *Data Rep. ERL AOML-34*, 163 pp., NOAA, Miami, Fla.

Pérez, F. F., M. Vasquez-Rodriguez, E. Louarn, X. A. Padin, H. Mercier, and A. F. Rios (2009), Temporal variability of the anthropogenic CO_2 storage in the Irminger Sea, *Biogeosciences*, *75*, 280–289.

Perigaud, C., and P. Delecluse (1992), Annual sea level variations in the southern tropical Indian Ocean from Geosat and shallow-water simulations, *J. Geophys. Res.*, *97*(C12), 20,169–20,178, doi:10.1029/92JC01961.

Raynaud, S., O. Aumont, K. B. Rodgers, P. Yiou, and J. C. Orr (2005), Interannual-to-decadal variability of North Atlantic air-sea CO_2 fluxes, *Ocean Sci.*, *2*, 43–60.

Rodgers, K. B., O. Aumont, G. Madec, C. Menkes, B. Blanke, P. Monfray, J. C. Orr, and D. P. Schrag (2004), Radiocarbon as a thermocline proxy for the eastern equatorial Pacific, *Geophys. Res. Lett.*, *31*, L14314, doi:10.1029/2004GL019764.

Rodgers, K. B., O. Aumont, C. Menkes, and T. Gorgues (2008a), Decadal variations in equatorial Pacific ecosystems and ferocline/pycnocline decoupling, *Global Biogeochem. Cycles*, *22*, GB2019, doi:10.1029/2006GB002919.

Rodgers, K. B., J. L. Sarmiento, O. Aumont, C. Crevoisier, C. de Boyer Montegut, and N. Metzl (2008b), A wintertime uptake window for Anthropogenic CO_2 in the North Pacific, *Global Biogeochem. Cycles*, *22*, GB2020, doi:10.1029/2006GB002920.

Sabine, C. L., et al. (2004), The ocean sink for anthropogenic CO_2, *Science*, *305*, 367–371, doi:10.1126/science.1097403.

Sabine, C. L., R. A. Feely, and R. Wanninkhof (2006), Global oceans: Ocean carbon, *Bull. Am. Meteorol. Soc.*, *87*(6), S29–S30.

Sabine, C. L., R. A. Fely, F. J. Millero, A. G. Dickson, C. Langdon, S. Mecking, and D. Greeley (2008), Decadal changes in Pacific carbon, *J. Geophys. Res.*, *113*, C07021, doi:10.1029/2007JC004577.

Stephens, C., J. I. Antonov, T. P. Boyer, M. E. Conkright, R. A. Locarnini, T. D. O'Brien, and H. E. Garcia (2002), *World Ocean Atlas 2001* [CD ROM], vol. 1, *Temperature*, *NOAA Atlas NESDIS*, vol. 49, 165 pp., Silver Spring, Md.

Tanhua, T., A. Körtzinger, K. Friis, D. W. Waugh, and D. W. R. Wallace (2007), An estimate of anthropogenic CO_2 inventory from decadal changes in oceanic carbon content, *Proc. Natl. Acad. Sci. U. S. A.*, *104*, 3037–3042, doi:10.1073/pnas.0606574104.

Wanninkhof, R., S. Doney, J. L. Bullister, N. Gruber, C. Sabine, R. A. Feely, G. C. Johnson, and F. Millero (2006), Changes in inorganic carbon inventory in the Atlantic Ocean over the last decade, *EOS Trans. AGU*, *87*(36), *Ocean Sci. Meet. Suppl.*, Abstract OS52C–01.

Wetzel, P., A. Winguth, and E. Maier-Reimer (2005), Sea-to-air CO_2 flux from 1948 to 2003: A model study, *Global Biogeochem. Cycles*, *19*, GB2005, doi:10.1029/2004GB002339.

Yamanaka, Y., N. Yoshie, M. Fujii, M. N. Aita, and M. J. Kishi (2004), An ecosystem model coupled with nitrogen-silicon-carbon cycles applied to Station A7 in the northwestern Pacific, *J. Oceanogr.*, *60*, 227–241, doi:10.1023/B:JOCE.0000038329.91976.7d.

O. Aumont, C. Lo Monaco, and N. Metzl, LOCEAN, IPSL, Université Pierre et Marie Curie, 4 Place Jussieu, F-75252 Paris CEDEX 05, France.

L. Bopp, LSCE, DSM, L'Orme des Merisiers, Bat 701, F-91191 Gif-sur-Yvette, France.

S. C. Doney and D. M. Glover, WHOI, 266 Woods Hole Road, Woods Hole, MA 02543, USA.

J. P. Dunne and A. Gnanadesikan, GFDL, NOAA, 201 Forrestal Road, Princeton, NJ 08540-6649, USA.

A. Ishida, IORGC, JAMSTEC, 3173-25 Showamachi, Yokohama 236-0001, Japan.

M. Ishii, MRI, 1-1 Nagamine, Tsukuba 305-0052, Japan.

A. R. Jacobson, CIRES, University of Colorado at Boulder, 216 UCB, Boulder, CO 80309-0216, USA.

R. M. Key, K. B. Rodgers, and J. L. Sarmiento, AOS Program, Princeton University, 300 Forrestal Road, 311 Sayre Hall, Princeton, NJ 08540, USA.

E. Maier-Reimer and P. Wetzel, MPI, Bundesstrasse 53, D-20146 Hamburg, Germany.

H. Mercier, LPO, IFREMER, IRD, UBO, CNRS, BP 75, F-29280 Plouzane, France.

F. F. Pérez and A. F. Rios, CSIC, Serrano 117, Madrid E-28006, Spain.

R. Wanninkhof, AOML, NOAA, 4301 Rickenbacker Causeway, Miami, FL 33149, USA.

C. D. Winn, College of Natural and Computational Sciences, Hawaii Pacific University, 45-045 Kamehameha Highway, Kaneohe, HI 97664, USA.

Y. Yamanaka, Graduate School of Environmental Earth Science, Hokkaido University, Sapporo 060-0810, Japan.